the diketone groups and the chelating atom of the adduct. A postulated intramolecular exchange mechanism has the adduct rise above this plane and rotate about the uranyl axis to the other side.[2b] If this mechanism is correct, one would expect a greater activation energy for intramolecular exchange the greater the distance of the uranium above the plane of the ligands. These distances and the activation energies are listed in Table IV. There is not good agreement between the two sets of parameters.

Another possible intramolecular exchange mechanism is the rotation of the β-diketone ring about an axis perpendicular to that of the uranyl group. This would have the effect of changing the positions of two, rather than all four, of the trifluoromethyl groups. It is reasonable to suppose that the more nearly planar the β-diketone ring the more easily it might rotate. In Table IV are listed the maximum deviations from planarity for a carbon in each of the β-diketone rings of the adduct. There is a good correlation between these deformations and the activation energy for trifluoromethyl exchange, except for the azide adduct. In this case it is not possible to determine which of the two isomers observed in solution is isolated in the solid. If it is the more rapidly averaging isomer, which would have a lower activation energy than that reported, then the correlation is good for all the compounds. It is therefore suggested that in these adducts the exchange occurs by rotation of the β-diketone ring.

Conclusions

Two different structural forms of the azide and fluoborate adducts coexist in sulfur dioxide solution. The higher energy form has a faster averaging for the trifluoromethyl groups in both adducts. There are two concurrent exchange mechanisms for the tetrahydrofuran and chloride adducts. The lower energy pathway is by an intermolecular displacement mechanism, and the higher energy one by an intramolecular exchange. In all the adducts the intramolecular exchange probably occurs by rotation of the β-diketone ring.

Acknowledgment. The authors wish to thank Dr. G. Kramer for some unpublished results and helpful comments. They greatly appreciate the determination of the crystal structures by Drs. E. Gabe and L. Prasad.

Registry No. Uranyl bis(hexafluoroacetylacetonate), tetrahydrofuran adduct, 69244-67-3; uranyl bis(hexafluoroacetylacetonate), chloride adduct, 83862-68-4; uranyl bis(hexafluoroacetylacetonate), azide adduct, 83876-04-4; uranyl bis(hexafluoroacetylacetonate), fluoroborate adduct, 83862-69-5; uranyl bis(hexafluoroacetylacetonate), perchlorate adduct, 83862-70-8; uranyl bis(hexafluoroacetylacetonate), bromide adduct, 83862-71-9; uranyl bis(hexafluoroacetylacetonate), trimethyl phosphate adduct, 64708-00-5.

Contribution from the Department of Chemistry, The University of North Carolina, Chapel Hill, North Carolina 27514

Hydrogen-Bonding-Induced Solvatochromism in the Charge-Transfer Transitions of Ruthenium(II) and Ruthenium(III) Ammine Complexes

JEFF C. CURTIS, B. PATRICK SULLIVAN, and THOMAS J. MEYER*

Received February 19, 1982

The ligand to metal and metal to ligand charge-transfer transitions in a variety of Ru(II) and Ru(III) polypyridyl–ammine complexes have been shown to be exceedingly solvent dependent. The solvatochromic behavior cannot be explained in terms of simple bulk dielectric properties of the solvents. Evidence is presented that specific solvent interactions between coordinated NH_3 and donor solvents change the redox asymmetry within the molecule (estimated as $\Delta E_{1/2} = E_{1/2}$(Ru donor) − $E_{1/2}$(polypyridine acceptor)) and that this is the principal contributor to the change in the CT band energies. It is also demonstrated that preferential outer-sphere solvation can be observed in binary solvent mixtures, the result being that the stronger donor solvent of the mixture is found in close proximity to the ion. Evidence is also presented for specific donor–acceptor effects in an ion pair involving the iodide ion.

Introduction

Many transition-metal complexes display solvatochromatic behavior resulting from the solvent dependence of the energies of visible charge-transfer absorption bands.[1-4] Solvatochromic behavior is not solely a property of charge-transfer transitions, and in fact subtle solvent effects on the d–d transitions of various Co(III) and Cr(III) complexes were investigated as early as 1956 by Bjerrum et al.[5] However, the majority of known cases involve transitions which are largely charge transfer in character. For example, Miller and Dance[6] have noted the strong solvent effects on the interligand charge-transfer transition in some mixed-ligand dithiolene complexes and have found that the observed solvatochromic shifts correlate with the gas-phase dipole moments of the various solvents employed. Burgess has demonstrated that the charge-transfer band maximum for the metal to 2,2′-bipyridine ligand transition, π^*(bpy) ← dπ, in such complexes as $[Fe^{II}(bpy)_2(CN)_2]$ and $[M(bpy)(CO)_4]$ (M = W, Mo), is influenced strongly by the solvent and correlates with the E_T solvent scale of Reichardt–Dimroth and the Z scale due to Kosower.[1,7,8] Similarly, Gidney et al. have correlated the solvatochromatism observed in the series of square-planar d^8 complexes $M^{II}(bpy)X_2$ (M = Pt, Pd; X = Cl, Br, I, py) with the E_T scale.[2,7]

Briefly, the E_T scale of Reichardt and Dimroth is an ordering of solvent polarity based on the position of the energy maximum for the intramolecular charge-transfer band in a pyridinium N-phenolbetaine molecule (see eq 1). The charge-transfer transition in the betaine is exceedingly solvent dependent, changing from 453 nm in water to 810 nm in diphenyl ether.

The Z scale of Kosower correlates roughly linearly with that of Reichardt and is also based on an organic charge-transfer transition involving a pyridinium site. In this case it is the

(1) (a) Burgess, J. *Spectrochim. Acta, Part A* **1970**, *A26*, 1369. (b) Burgess, J. *J. Organomet. Chem.* **1969**, *19*, 218. (c) Burgess, J. *Spectrochim. Acta, Part A* **1970**, *A26*, 1957.
(2) Gidney, P. M.; Gillard, R. D.; Heaton, B. T. *J. Chem. Soc., Dalton Trans.* **1973**, 132.
(3) Kober, E. M.; Sullivan, B. P.; Meyer, T. J., manuscript in preparation.
(4) Ford, P. C.; Rudd, D. P.; Gaunder, R.; Taube, H. *J. Am. Chem. Soc.* **1968**, *90*, 1187.
(5) Bjerrum, Jannik; Adamson, A. W.; Bostrup, Ole. *Acta Chem. Scand.* **1956**, *10*, 329.
(6) Miller, T. R.; Dance, I. G. *J. Am. Chem. Soc.* **1973**, *95*, 6970.
(7) Reichardt, C. *Angew. Chem., Int. Ed. Engl.* **1965**, *4*, 29.

0020-1669/83/1322-0224$01.50/0

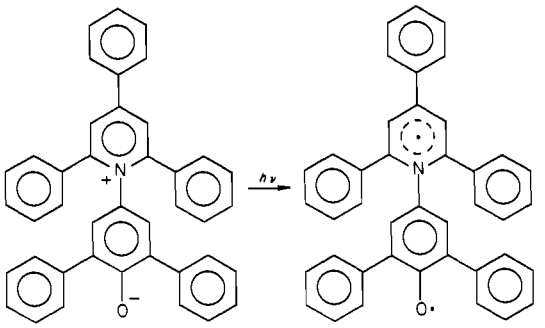

(1)[7]

intermolecular ion-pair charge transfer between the *N*-ethyl-4-carbomethoxypyridinium cation and the iodide anion[8] (eq 2).

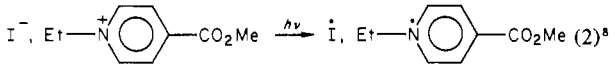

(2)[8]

Although these scales are useful[7] in many contexts and often correctly predict solvent-dependent trends in the rates of such diverse chemical processes as Diels–Alder reactions, organic rearrangements, and solvolysis reactions, they are of limited conceptual value in that they are not simply related to any single intrinsic solvent property that is interpretable on the molecular level such as dielectric constant, refractive index, or dipole moment. Most importantly, there is no theoretical basis at the microscopic level for understanding the origin of such scales.

A form of solvatochromism that has been studied in some detail involves the solvent dependence of metal–metal charge-transfer (MMCT) or intervalence-transfer (IT) transitions between redox sites in mixed-valence transition-metal dimers; e.g., eq 3 (bpy is 2,2′-bipyridine).[9-12] In eq 3 the

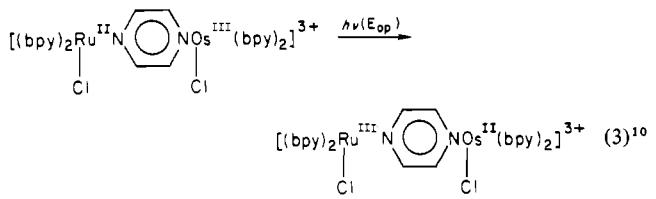

(3)[10]

charge distribution produced upon optical electron transfer corresponds to a high-energy oxidation state or electronic isomer. Because of the Franck–Condon principle, the oxidation state isomer is formed initially in nonequilibrium vibrational levels with respect to the intramolecular and medium vibrations. For these systems it has been convincingly demonstrated that, with an appropriate choice of solvents, to a first approximation the energy of the optical transition, E_{op}, varies directly as a simple function of the bulk dielectric properties of the medium[12] as shown in eq 4. Equation 4 has a firm theoretical basis from electron-transfer and dielectric continuum theory.[12,13] In eq 4, ΔE is the thermodynamic energy

$$E_{op} = \Delta E + \chi_{inner} + \chi_{outer} = \Delta E + \chi_i + \chi_o \qquad (4)$$

difference between the equilibrium vibrational states of the two different redox isomers, χ_i is the contribution to the Franck–Condon energy for the transition due to the intramolecular, inner-coordination sphere vibrations, and χ_o is the contribution to the Franck–Condon energy due to the collective vibrations of the medium. In the classical limit, on the assumption that the medium can be treated as a dielectric continuum, χ_o is given by eq 5, where D_{op} and D_s are the optical

$$\chi_o = \frac{1}{2}\left(\frac{1}{D_{op}} - \frac{1}{D_s}\right)\int (\hat{E}_f - \hat{E}_i)^2 dV \qquad (5)[13]$$

and static dielectric constants of the medium and $\hat{E}_f$ and $\hat{E}_i$ are the electric field vectors of the charge distributions after and before electron transfer in the absence of the medium. Integration of eq 5 for the case of spherical nonpenetrating electron-donor and -acceptor sites, neglecting the volume of the sites, gives eq 6, where a_1 and a_2 are the radii of the sites, d is the intermolecular distance between them, and e is the unit electron charge.

$$\chi_o = e^2\left(\frac{1}{2a_1} + \frac{1}{2a_2} - \frac{1}{d}\right)\left(\frac{1}{D_{op}} - \frac{1}{D_s}\right) \qquad (6)[13]$$

Early in the development of ruthenium ammine chemistry, Ford et al. noted that there was a strong solvent dependence for the MLCT band in the ruthenium(II) pentammine pyridine ion[4] (see eq 7). At the time of the observation, however, no

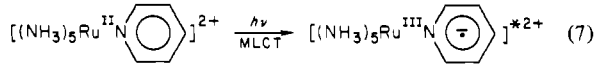

(7)

detailed explanation was offered for the observed solvent effects.

The work reported here was undertaken with the goal of understanding the origins of the solvatochromism for MLCT transitions in a series of Ru(II) ammine complexes like those shown in eq 7–9

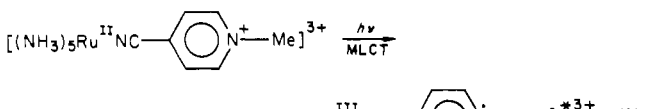

(8)

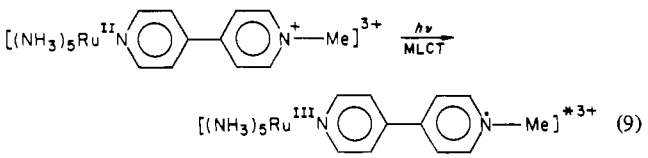

(9)

and in ions of Ru(III) like

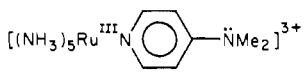

where the transition is a ligand to metal charge-transfer (LMCT) process.

Experimental Section

Solvents. Nitromethane, acetonitrile, *N*,*N*-dimethylacetamide, *N*,*N*-dimethylformamide, dimethyl sulfoxide, and **benzonitrile** were all obtained as Gold Label spectrophotometric grade solvents from Aldrich and used without further purification. Purified **tri-*n*-butyl phosphate** was purchased from Fisher Scientific Co. and used without further purification. **Hexamethylphosphoramide** was purchased from Eastman and used as received. **Propylene carbonate** (1,2-propanediol cyclic carbonate) was purchased from Aldrich and vacuum distilled once taking the middle cut. **Cyclopentanone** was purchased from Eastman and used as received. Chromoquality ***N*-methylformamide** was obtained from Matheson Coleman and Bell and used without further purification. Reagent grade **acetone** was purchased from Mallinckrodt and used without further purification.

Most solvents were allowed to stand at least overnight over 3-Å molecular sieves (Davison Chemical) in order to remove trace water before use in spectrophotometric experiments.

(8) Kosower, E. M. *J. Am. Chem. Soc.* **1958**, *80*, 3253.
(9) Powers, M. J.; Meyer, T. J. *J. Am. Chem. Soc.* **1980**, *102*, 1289.
(10) Sullivan, B. P.; Kober, E. M.; Meyer, T. J., manuscript in preparation.
(11) (a) Tom, G. M.; Creutz, C.; Taube, H. *J. Am. Chem. Soc.* **1974**, *96*, 7827. (b) Creutz, C. *Inorg. Chem.* **1978**, *17*, 3723.
(12) Sullivan, B. P.; Curtis, J. C.; Kober, E. M. *Nouv. J. Chim.* **1980**, *4*, 643.
(13) (a) Marcus, R. A. *J. Chem. Phys.* **1956**, *24*, 966. (b) Hush, N. S. *Electrochim. Acta* **1968**, *13*, 1005.

Electrochemical Measurements. The $E_{1/2}$ values were obtained as the half-point potentials between the oxidative and reductive current–voltage peak maxima from standard cyclic voltammograms recorded at 200 mV/s sweep rate by using a PAR Model 174 potentiostat and a house-designed signal generator. For cathodic work the electrolyte solutions were dried over 3-Å molecular sieves and purged of oxygen by nitrogen bubbling.

Due to the poor solubility characteristics of some of the pentaammineruthenium ions as perchlorate salts in polar organic solvents, the electrolyte used was 0.1 M tetra-*n*-butylammonium hexafluorophosphate (TBAH) rather than the corresponding perchlorate. The major portion of the electrochemical work was done in acetonitrile (Burdick and Jackson) on a polished Pt-disk electrode. For those potentials that were measured in water a polished gold-disk electrode was employed and the ionic strength of the solutions was adjusted to 0.1 M with 0.09 M NaTFA (Aldrich) and a 0.01 M HOAc–NaOAc pH 5 buffer.

Preparation of the Pyridinium Ligands. *N*-Methyl-4,4′-bipyridinium iodide, [*N*-Me-4,4′-bpy]I was synthesized in the following manner: Three grams of 4,4′-bipyridine dihydrate (Aldrich) was stirred in 100 mL of anhydrous diethyl ether and 5 mL of neat methyl iodide. The reaction was allowed to proceed at room temperature for 3 days, at which time the crude yellow solid [*N*-Me-4,4′-bpy]I was isolated by filtration and washed extensively with ether: yield ~2 g, 40%. The purity of this material (specifically, the absence of the dimethylated product) was verified by cyclic voltammetry, which showed only *one* reductive wave between 0 and −1.2 V centered at −0.96 V. The iodide salt was metathesized to the chloride by simply dissolving a portion of the iodide salt into a minimum volume of acetone and then adding an excess of tetrabutylammonium chloride in acetone solution. The white, hygroscopic precipitate, [N-Me-4,4′-bpy]Cl was isolated by filtration and stored under vacuum.

4-Cyano-*N*-methylpyridinium iodide, [4-CN-*N*-Mepyd]I was obtained as a preexisting sample from the work of Dr. J. K. Nagle and used without further purification.[14]

Preparation of the Ruthenium Complexes. $[Ru(bpy)_3](BF_4)_2$ was obtained as a preexisting sample from J. K. Nagle[14] and checked spectrally to verify purity. $[Ru(bpy)_2(NH_3)_2](PF_6)_2$ was obtained as a preexisting sample from the work of J. L. Cramer[15] and purified by partial reprecipitation (vide infra) from acetonitrile and ether. $[Ru^{III}(NH_3)_5Cl]Cl_2$ was synthesized according to a literature method.[16] $[Ru(NH_3)_5(OH_2)](PF_6)_2$ was synthesized via a modification of the method of Baumann.[17] In a typical preparation, 0.2 g of $[Ru(NH_3)_5Cl]Cl_2$ (6.68 mmol) was reduced over ~1 g of Zn–Hg amalgam in 5 mL of H_2O slightly acidified with 1–2 drops of trifluoroacetic acid for about 30 min, or until all of the ruthenium(III) chloropentaammine starting material had dissolved and reacted to form the pale yellow ruthenium(II) aquopentaammine ion. The solution was agitated during this reduction period by bubbling purified argon gas up through the frit supporting the Zn–Hg amalgam. Care was taken not to allow the reduction step to proceed past ~45 min, as the $[Ru^{II}(NH_3)_5OH_2]^{2+}$ in solution began to degrade past that point, yielding a dark greenish solution. Upon completion of the reduction step, the solution of $[Ru^{II}(NH_3)_5(OH_2)]^{2+}$ was allowed to drip down into a stirred solution of saturated $(NH_4)PF_6$ below (~5 mL). This caused the immediate precipitation of the pale yellow product $[Ru^{II}(NH_3)_5(OH_2)](PF_6)_2$, which was collected by filtration under a blanket of argon, washed with a 20–80% mixture of ethanol–ether, and stored under vacuum (any exposure to O_2 while the product is wet with water will result in the formation of deep red, oxo-bridged impurities). Typical yields were on the order of 60–80%. In the best cases the product was obtained as a pale yellow powder although samples with a slight greenish or tan color are often obtained, which serve adequately for further transformations. Elemental analyses obtained for the $[Ru(NH_3)_5(OH_2)](PF_6)_2$ samples thus obtained are less than ideal [e.g., calcd (obsd): C, 0 (0.30); H, 3.47 (2.94); N, 14.11 (12.50)], but the lack of analytical purity did not appear to influence the synthetic utility of the samples.

$[Ru(bpy)(NH_3)_4](PF_6)_2$. A 0.21-g (0.43-mmol) sample of $[Ru(NH_3)_5(OH_2)](PF_6)_2$ was dissolved in 40 mL of argon-degassed acetone (N_2 degassing causes the formation of the dinitrogen complex, which competes with the desired reaction), forming an orange solution of the $[Ru(NH_3)_5(CH_3COCH_3)]^{2+}$ ion. To this was added 0.07 g of 2,2′-bipyridine, and the solution was allowed to stir at room temperature under a blanket of argon for 8 h. The crude purple-red $[Ru(bpy)(NH_3)_4](PF_6)_2$ product was collected by simply filtering the reaction mixture (now passivated toward O_2) into 6 volumes of stirring ether and filtering off the product, 0.12 g, 55%. This material was purified in the following manner: The crude product was dissolved in a minimum volume (ca. 4 mL) of either spectroquality or reagent grade acetone and cooled to 0 °C in the freezer. On top of this was then carefully layered 2–3 mL of anhydrous ether, or until turbidity just started to occur in the upper part of the acetonitrile layer. The resulting double-layered system was allowed to stand quietly and mix by diffusion at 0 °C for at least 12 h, at which point more ether was added if no solid had precipitated. For optimum purity, a recovery of no more than 40–50% was attempted. A second crop of reasonable quality could be obtained by repeating this procedure on the mother liquor after the first crop of dark, semicrystalline material had been collected.

$[Ru^{II}(NH_3)_5(L)](PF_6)_{2,3}$ (L = Pyridine (py), 4-Cyano-*N*-methylpyridinium (4-CN-*N*-Mepyd), or *N*-Methyl-4,4′-bipyridine (*N*-Me-4,4′-bpy)). A 0.2-g sample of $[Ru^{III}(NH_3)_5Cl]Cl_2$ starting material in 5 mL of H_2O was reduced with argon-bubbling agitation for 30 min and then allowed to drop down into an argon-degassed solution of 1.2 equi of the ligand, L, in 10 mL of water. After 2 h the crude $[Ru^{II}(NH_3)_5(L)](PF_6)_{2,3}$ product was precipitated by adding 5 mL of a saturated solution of $(NH_4)PF_6$ in water. Yields were typically 60–70% and the solids thus obtained were purified by using the partial reprecipitation method described for the $[Ru^{II}(NH_3)_4(bpy)](PF_6)_2$ salt.

***trans*-$[L(NH_3)_4Ru^{II}L'](PF_6)_3$ (L = Pyridine, 3-Chloropyridine, 3,5-Dichloropyridine; L′ = 4-Cyano-*N*-methylpyridinium, *N*-Methyl-4,4′-bipyridine).** These compounds were synthesized similarly to the method of Isied and Taube[18] with starting materials made via the route of Ford and Clarke.[16b]

***trans*-$[SO_2(NH_3)_4Ru^{II}Cl]Cl$** was synthesized in the following manner: A 2.5-g (8.5-mmol) sample of $[(NH_3)_5Ru^{III}Cl]Cl_2$ was heated at 80 °C in a solution of 100 mL of water and 3.55 g (2.4 mmol) of $NaHSO_3$ (Matthey Bishop) for approximately 90 min. A continuous stream of SO_2 gas was bubbled through the solution during this period. Upon cooling to 0 °C, the solution deposited pale yellow crystals of *trans*-$[(NH_3)_4Ru^{II}(HSO_3)_2]$, which were collected by filtration, washed with acetone, and dried in vacuo. The yield was 1.9 g (67%). This material was then heated at reflux for 20 min in 200 mL of 6 M HCl, which upon cooling gave 1.4 g of orange, crystalline *trans*-$[(SO_2)Ru(NH_3)_4Cl]Cl$ (80% yield). This product was recrystallized once by dissolving it in a minimum volume (~75 mL) of hot 0.01 M HCl and filtering it while still hot into 25 mL of 1 M HCl. Anal. Calcd for $[Ru(NH_3)_4(SO_2)(Cl)]Cl\cdot 2H_2O$: H, 3.92; N, 18.18. Found: H, 3.83; N, 18.02.

***trans*-$[SO_4Ru^{III}(NH_3)_4(L)]Cl$ (L = py, 3-Cl-py, 3,5-Cl_2py).** In a typical preparation, 0.1 g (0.3 mmol) of *trans*-$[(SO_2)Ru(NH_3)_4Cl]Cl$ was dissolved in 5 mL of neutral H_2O at ~40 °C and a fivefold molar excess of L, in this case pyridine (0.13 mL, 1.5 mmol), was added and the solution was stirred for 15 min or until the color change was complete (orange → yellow). In the case of L = 3,5-Cl_2py, 1.0 mL of acetone was added during this step in order to enhance the solubility of the ligand. After the substitution was complete, the product *trans*-$[(SO_2)Ru^{II}(NH_3)_4(L)]Cl_2$ was precipitated by the addition of 15 volumes of acetone collected by filtration, washed with acetone and ether, and dried in vacuo. This solid was then dissolved in a minimum volume (~5 mL) of neutral H_2O and filtered into a small Erlenmeyer flask. To this solution was slowly added 3 mL of an oxidizing solution consisting of a 1:1 mixture of 30% H_2O_2 and 2 N HCl. This solution was stirred for approximately 10 min to ensure complete reaction. The yellow product, *trans*-$[SO_4Ru^{III}(NH_3)_5(py)]Cl$,

(14) Nagle, J. K. Ph.D. Dissertation, The University of North Carolina, Chapel Hill, 1979.
(15) Cramer, J. L. Ph.D. Dissertation, The University of North Carolina, Chapel Hill, 1975.
(16) (a) Vogt, L. H.; Katz, J. S.; Wiberly, S. E. *Inorg. Chem.* **1965**, *4*, 1156. (b) Clarke, R. E. Masters Thesis, The University of California, Santa Barbara, CA, 1978.
(17) Baumann, J. A. Ph.D. Thesis, The University of North Carolina, Chapel Hill, 1978.
(18) (a) Isied, S. S.; Taube, H. *Inorg. Chem.* **1974**, *13*, 1545. (b) Isied, S. S.; Taube, H. *Ibid.* **1976**, *15*, 3070.
(19) (a) Gutmann, V. *Electrochim. Acta* **1976**, *21*, 661. (b) Gutmann, V. "The Donor-Acceptor Approach to Molecular Interactions"; Plenum Press: New York, 1978.

was then precipitated by the addition of 15 volumes of acetone, collected by filtration, and dried in vacuo. The yield for L = pyridine was 0.098 g, 78%. Yields for the cases L = 3-Cl-py and 3,5-Cl_2py were slightly less.

***trans*-[(L)$Ru^{II}(NH_3)_4$(L')](PF$_6$)$_{2,3}$ (L = py, 3-Cl-py, 3,5-Cl_2py; L' = 4-Cyano-*N*-methylpyridinium, *N*-Methyl-4,4'-bipyridine).** In a typical synthesis, 0.1 g of *trans*-[$SO_4Ru^{III}(NH_3)_4$(L)]Cl was reduced in 5 mL of H_2O over ~1.0 g Zn–Hg amalgam with continuous agitation via argon bubbling for 30 min. The orange solution of *trans*-[$(H_2O)Ru^{II}(NH_3)_4$(L)]$^{2+}$ (the ruthenium(II) sulfato complex may also be present) was added to a degassed solution of a 20% molar excess of the ligand L' (chloride or iodide salts) in 10 mL of water. The red-purple color of the product developed over a period of minutes for L = py but required much longer times for L = 3-Cl-py and 3,5-Cl_2py. The reaction was allowed to proceed under a blanket of argon for at least 2 h in the case of L = py and 6 h or longer when L = 3-Cl-py and 3,5-Cl_2py. The substitution reaction to form the complexed pyridinium products was much slower and less efficient for these latter two cases, and the purities of the obtained products were substantially less. This probably indicates that, as electron density at the Ru^{II} center is depleted by more and more electron-withdrawing power on the pyridine ligand, the trans site becomes less labile toward substitution.

After the substitution was deemed complete, the crude trans-substituted product was precipitated via the addition of 5 mL of saturated $(NH_4)(PF_6)$ in water. The solid was isolated by filtration, washed sparingly with cold water, and dried in vacuo. The yields when L = py were 50–60%, and when L = 3-Cl-py and 3,5-Cl_2py, the yields fell to 30–40%. The crude products were freed of insoluble impurities by dissolving them in acetone and then filtering them into 15 volumes of stirring anhydrous ether. The resulting solids were collected by filtration and then further purified via the partial reprecipitation method described previously. The analytical data for these and the other compounds used in this study are presented in Table I. As can be seen, the analyses for the trans species with 3-Cl-py and 3,5-Cl_2py are in some cases less than ideal. Electrochemical and spectroscopic data obtained on these compounds, however, were reproducible and sensible as long as the experiments were carried out within several days of their preparation and isolation.

[$Ru^{II}(NH_3)_5$(L)](PF$_6$)$_2$ (L = 4-(Dimethylamino)benzonitrile (dmabn), 4-(Dimethylamino)pyridine (dmapy)). These complexes were synthesized from the aquopentaammine starting material. In a typical preparation, 0.10 g of [$Ru^{II}(NH_3)_5(OH_2)$](PF$_6$)$_2$ was dissolved in 50 mL of argon-degassed acetone, yielding an orange solution of the [$Ru^{II}(NH_3)_5(CH_3COCH_3)$]$^{2+}$ ion. To this was then added a threefold molar excess of the appropriate ligand L. The solution was allowed to stir at room temperature under a blanket of argon for at least 2 h, at which time the product was isolated by reducing the volume to ca. 10 mL on a rotary evaporator and then filtering the solution into 10 volumes of stirring anhydrous ether. The solid product was then collected by filtration, washed with ether, and dried in vacuo. The solids thus obtained were very oxygen sensitive, especially in the case of the 4-(dimethylamino)pyridine ligand.

These compounds appeared to undergo fairly rapid solid-state decomposition in both the II and the III oxidation states. However, they gave clean, reversible electrochemistry and in their ruthenium(III) oxidative states gave clean, Gaussian-shaped ligand-to-metal charge-transfer bands (LMCT).

For the solvatochromatic studies of the LMCT bands of the Ru(III) complexes, the oxidized forms were generated in situ by the addition of a small amount of bromine vapor to a solution of the ruthenium(II) complex dissolved in the solvent in question. It was possible to isolate the ruthenium(III) compounds by dissolving a small amount of the Ru(II) PF_6 salt in acetone, precipitating it as the chloride via the addition of several milliliters of saturated tetra-*n*-butylammonium chloride in acetone, collecting the [$Ru^{II}(NH_3)_5$(L)]Cl_2 product by filtration, dissolving it in a minimum of 0.2 M HCl, and then oxidizing the Ru(II) to Ru(III) by the dropwise addition of 30% H_2O_2. The brightly colored [$Ru^{III}(NH_3)_5$(L)]Cl_3 product (deep blue for L = dmapy; turquoise for L = dmabn) was then precipitated via the addition of 10 volumes of acetone, collected by filtration, and dried in vacuo.

Spectrophotometric Measurements. The spectra were obtained predominantly on a Cary 17 recording spectrophotometer, although some measurements were made on a Bausch & Lomb UV-210 spectrophotometer. The wavelength accuracy of the λ_{max} values is taken to be ~2 nm, independent of spectral range.

All spectra were run with use of a matched cell filled with the appropriate solvent in the reference compartment. This was critically important in obtaining accurate and reproducible λ_{max} values.

Table I. Structures and Abbreviations for the Ligands Used in This Study

ligand	name	abbreviation
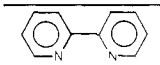	2,2'-bipyridine	bpy
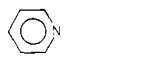	pyridine	py
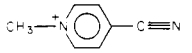	4-cyano-*N*-methylpyridinium	4-CN-*N*-Mepyd
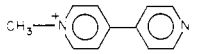	*N*-methyl-4,4'-bipyridine	*N*-Me-4,4'-bpy
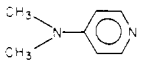	4-(dimethylamino)-pyridine	dmapy
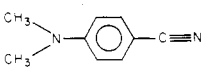	4-(dimethylamino)-benzonitrile	dmabn
	3-chloropyridine	3-Cl-py
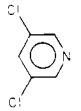	3,5-dichloropyridine	3,5-Cl_2py
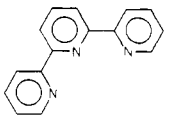	2,2',2''-terpyridine	trpy

Results

Nature and Properties of the Complexes Used in the Solvatochromism Studies. The structures and abbreviations for the ligands used in our study are given in Table I, and elemental analyses for the new complexes are shown in Table II. As mentioned in the Introduction, dramatic solvent effects were observed for the π^*(py) ← dπ(Ru) CT transition in $Ru^{II}(NH_3)_5py^{2+}$ by Ford et al.[4] This interesting observation, coupled with earlier successes at interpreting solvent effects on MMCT bands in mixed-valence dimers through the use of simple dielectric continuum theory, led us to prepare and study the solvatochromic behavior of the CT transitions in five series of complexes: (1) mixed ammine 2,2'-bipyridyl complexes $Ru^{II}(bpy)_3^{2+}$, $Ru^{II}(bpy)_2(NH_3)_2^{2+}$, and $Ru^{II}(bpy)(NH_3)_4^{2+}$; (2) pentaammine pyridine and pyridinium complexes $Ru^{II}(NH_3)_5py^{2+}$, [$Ru^{II}(NH_3)_5$(4-CN-*N*-Mepyd)]$^{3+}$, and [$Ru(NH_3)_5$(*N*-Me-4,4'-bpy)]$^{3+}$; (3) *trans*-tetraammine pyridinium complexes *trans*-[$Ru^{II}(NH_3)_4$(L)(4-CN-*N*-Mepyd)]$^{3+}$, and *trans*-[$Ru^{II}(NH_3)_4$(L)(*N*-Me-4,4'-bpy)]$^{3+}$ where L = py, 3-Cl-py; (4) mixed 2,2',2''-terpyridine complexes Ru(trpy)(bpy)$(NH_3)^{2+}$ and Ru(trpy)$(NH_3)_3^{2+}$; and (5) Ru(III) ammine complexes with ligand-based electron donor sites [$Ru^{III}(NH_3)_5$(4-CN-*N*,*N*-Me_2py)]$^{3+}$ and [$Ru^{III}(NH_3)_5$(4-($\ddot{N}Me_2$)py)]$^{3+}$ where the optical transition in the visible is now ligand to metal (LMCT) in character, for example

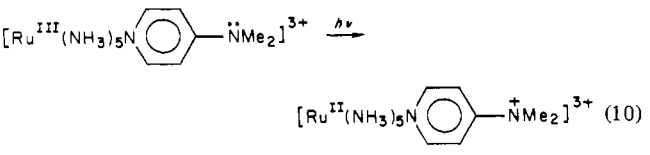

(10)

The synthesis of these complexes was accomplished, in most cases, by modification of literature methods, and the details

Table II. Elemental Analysis Data for the Complexes Used in the Spectroscopic Studies

compd	% by anal., calcd (obsd)		
	C	H	N
$[Ru(bpy)(NH_3)_4](PF_6)_2$	19.52 (20.03)	3.28 (2.30)	13.66 (12.87)
$[Ru(NH_3)_5(py)](PF_6)_2$	10.81 (11.14)	3.63 (3.41)	15.13 (14.60)
$[Ru(NH_3)_5(4\text{-CN-}N\text{-Mepyd})](PF_6)_3$	11.36 (11.59)	2.99 (2.88)	13.24 (13.04)
trans-$[(py)Ru(NH_3)_4(4\text{-CN-}N\text{-Mepyd})](PF_6)_3 \cdot H_2O$	17.57 (17.84)	3.56 (2.70)	11.95 (11.88)
trans-$[(3\text{-Cl-py})Ru(NH_3)_4(4\text{-CN-}N\text{-Mepyd})](PF_6)_3 \cdot H_2O$	16.86 (16.71)	2.95 (2.59)	11.47 (11.62)
trans-$[(3,5\text{-}Cl_2py)Ru(NH_3)_4(4\text{-CN-}N\text{-Mepyd})](PF_6)_3$	16.50 (14.50)	2.55 (1.91)	11.25 (12.16)
$[Ru(NH_3)_5(N\text{-Me-}4,4'\text{-bpy})](PF_6)_3 \cdot H_2O$	16.30 (16.32)	3.48 (3.38)	12.10 (12.37)
trans-$[(py)Ru(NH_3)_4(N\text{-Me-}4,4'\text{-bpy})](PF_6)_3 \cdot H_2O$	22.02 (21.90)	3.46 (3.45)	11.24 (11.48)
trans-$[(3\text{-Cl-py})Ru(NH_3)_4(N\text{-Me-}4,4'\text{-bpy})](PF_6)_3 \cdot CH_3COCH_3$	24.10 (24.04)	3.51 (3.06)	10.35 (9.87)
trans-$[(3,5\text{-}Cl_2)pyRu(NH_3)_4(N\text{-Me-}4,4'\text{-bpy})](PF_6)_3$	20.81 (21.61)	2.84 (2.10)	10.61 (10.07)
$[Ru(NH_3)_5(dmabn)](PF_6)_2 \cdot 2H_2O$	16.41 (15.73)	4.43 (4.36)	14.89 (14.93)
$[Ru(NH_3)_5(dmabn)]Cl_3 \cdot H_2O$	24.60 (20.10)	5.70 (5.64)	22.34 (19.92)
$[Ru(NH_3)_5(dmapy)](PF_6)_2 \cdot 2H_2O$	13.25 (11.06)	4.21 (3.78)	15.45 (15.64)
$[Ru(NH_3)_5(dmapy)]Cl_3 \cdot H_2O$	19.42 (15.15)	6.29 (5.68)	22.66 (21.30)

Table III. Summary of Ultraviolet-Visible Spectra in Acetonitrile Solution

compd	λ_{max}, nm (ϵ_{max}, M^{-1} cm^{-1})
$[Ru^{II}(bpy)_3](PF_6)_2$	450 (1.42×10^4)
$[Ru^{II}(bpy)_2(NH_3)_2](ClO_4)_2$	243 (2.3×10^4)
	295 (7.0×10^4)
	346 (8.7×10^3)
	489 (1.1×10^4)
$[Ru^{II}(bpy)(NH_3)_4](PF_6)_2$	246 (1.07×10^4)
	295 (3.3×10^4)
	366 (6.38×10^3)
	525 (3.95×10^3)
$[Ru^{II}(NH_3)_5py](PF_6)_2$	243 (5.65×10^3)
	407 (7.74×10^3)
$[Ru^{II}(NH_3)_5(4\text{-CN-}N\text{-Mepy})](PF_6)_3$	233 (1.55×10^4)
	260 (1.57×10^4)
	543 (1.85×10^4)
trans-$[(py)Ru^{II}(NH_3)_4(4\text{-CN-}N\text{-Mepy})](PF_6)_3$	240 (1.80×10^4)
	267 (sh)
	275 (sh)
	338 (7.29×10^3)
	524 (2.02×10^4)
trans-$[(3\text{-Cl-py})Ru^{II}(NH_3)_4(4\text{-CN-}N\text{-Mepy})](PF_6)_3$	218 (1.6×10^4)
	232 (1.7×10^4)
	242 (1.8×10^4)
	276 (sh)
	354 (5.9×10^3)
	516 (2.1×10^4)
trans-$[(3,5\text{-}Cl_2py)Ru^{II}(NH_3)_4(4\text{-CN-}N\text{-Mepyd})](PF_6)_3$	235 (2.24×10^4)
	260 (2.23×10^4)
	504 (2.03×10^4)
$[Ru^{II}(NH_3)_5(N\text{-Me-}4,4'\text{-bpy})](PF_6)_3$	245 (1.78×10^4)
	584 (1.61×10^4)
trans-$[(py)Ru^{II}(NH_3)_4(N\text{-Me-}4,4'\text{-bpy})](PF_6)_3$	253 (2.03×10^4)
	266 (sh)
	374 (4.83×10^3)
	558 (1.47×10^4)
trans-$[(3\text{-Cl-py})Ru^{II}(NH_3)_4(N\text{-Me-}4,4'\text{-bpy})](PF_6)_3$	258 (2.0×10^4)
	393 (3.1×10^3)
	549 (1.1×10^4)
trans-$[(3,5\text{-}Cl_2py)Ru^{II}(NH_3)_4(N\text{-Me-}4,4'\text{-bpy})](PF_6)_3$	261 (2.70×10^4)
	585 (2.01×10^4)
$[Ru^{II}(NH_3)_5(dmabn)](PF_6)_3$	224 (1.2×10^4)
	240 (8.0×10^3)
	287 (1.84×10^4)
	342 (1.82×10^4)

are presented in the Experimental Section.

In Table III are summarized the important features of the UV–vis spectra for the complexes in CH_3CN solution. The feature of interest in the visible region is the lowest energy transition, which in all cases is assignable to either an MLCT (pyridine, polypyridine, or pyridinium acceptor) or an LMCT dimethylamino-to-Ru(III)) optical transition. In the complexes of the type *trans*-$(L)Ru(NH_3)_4L'^{2+}$ an additional MLCT transition occurs at higher energy, which is assigned as an MLCT transition involving the second ligand as acceptor. Figure 1 shows the multiple MLCT bands for several of the trans complexes.

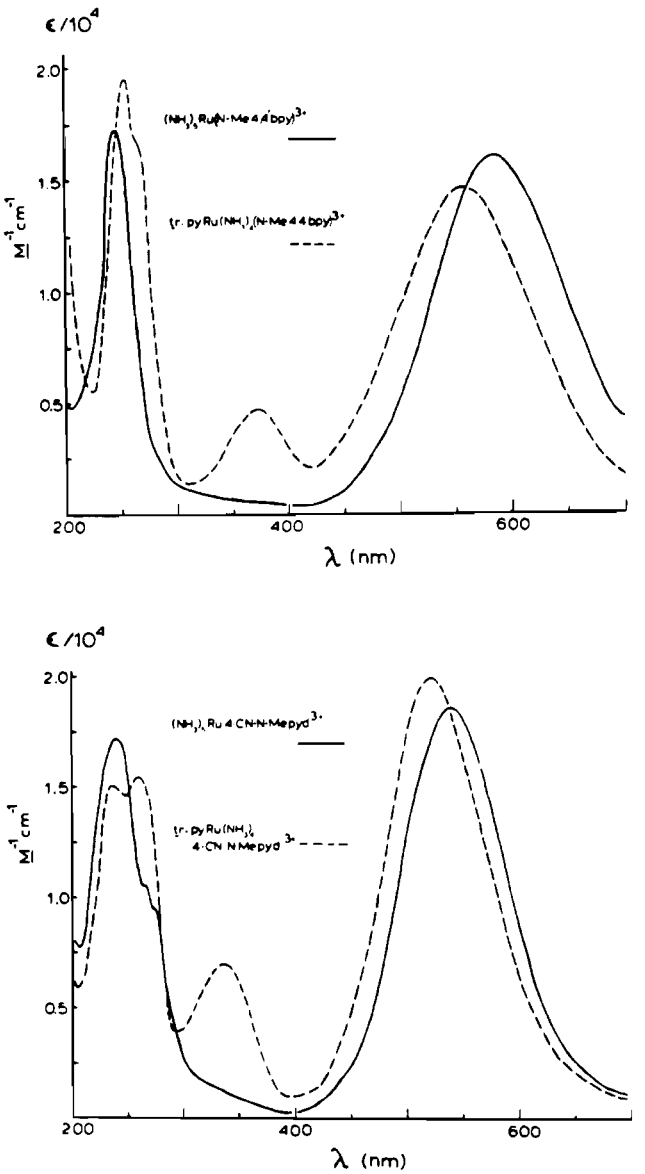

Figure 1. Spectra (ϵ vs. λ plots) in acetonitrile: (top) $[(NH_3)_5Ru(N\text{-Me-}4,4'\text{-bpy})]^{3+}$ and *trans*-$[(py)Ru(NH_3)_4(N\text{-Me-}4,4'\text{-bpy})]^{3+}$; (bottom) $[(NH_3)_5Ru(4\text{-CN-}N\text{-Mepyd})]^{3+}$ and *trans*-$[(py)Ru(NH_3)_4(4\text{-CN-}N\text{-Mepyd})]^{3+}$.

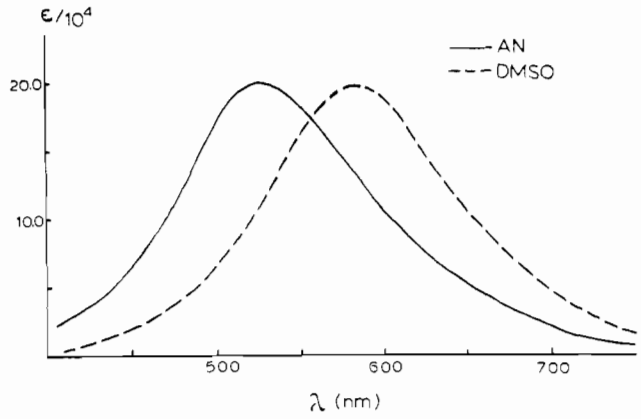

Figure 2. MLCT absorption band for $[(NH_3)_5Ru^{II}(4\text{-CN-}N\text{-Me-pyd})]^{3+}$ in acetonitrile and dimethyl sulfoxide.

Cyclic voltammetry in CH_3CN with $[N(n\text{-}C_4H_9)_4]PF_6$ as supporting electrolyte of the complexes showed reversible Ru^{III}/Ru^{II} couples as judged by the near-unity ratio of cathodic to anodic peak currents. The waves associated with ligand redox couples were also usually reversible, notable exceptions being the $-NMe_2$ oxidations, which had broad, ill-defined irreversible waves. The electrochemical data are given in Table IV, where the $E_{1/2}$ values are the average of oxidative and reductive peak potentials, $E_{1/2} = (E_{p,a} + E_{p,c})/2$.

Variations in MLCT Band Energies with Solvent. The profound difference that solvent can play on CT band energies in Ru(II) ammine complexes is illustrated in Figure 2 for $[(NH_3)_5Ru^{II}4\text{-CN-}N\text{-Mepy}]^{2+}$ where the spread in band energy difference as a function of solvent is ca. 1300 cm^{-1}. Table V gives E_{op} values for the complexes $(NH_3)_5Ru(py)^{2+}$, $(NH_3)_5RuL^{3+}$, and *trans*-$[(py)Ru(NH_3)_4L]^{3+}$ (L = 4-CN-*N*-Mepyd or *N*-Me-4,4′-bpy), in a series of solvents. The data presented in Table V are notable for the *absence* of hydroxylic solvents like water or methanol. A significant part of the Discussion is devoted to an interpretation of the observed solvent effects. The treatment developed is *not* applicable to hydroxylic solvents, and the quantitative details of the origin of their effects on CT bands are currently under investigation.

Table VI gives data of the same kind for the complexes $Ru(bpy)_3^{2+}$, $Ru(bpy)_2(NH_3)_2^{2+}$, $Ru(bpy)(NH_3)_4^{2+}$, $Ru(trpy)(bpy)(NH_3)^{2+}$ (trpy is 2,2′,2″-terpyridine), and $Ru(trpy)(NH_3)_3^{2+}$ and Table VII for the LMCT (ligand to metal charge transfer) bands in $(NH_3)_5Ru^{III}(dmabn)^{3+}$ and $(NH_3)_5Ru^{III}(dmapy)^{3+}$. Details of the preparations and properties of the trpy complexes will be reported in a separate paper.[20] The MLCT spectra for the trpy complexes are somewhat more complex than related bpy complexes because of the more complicated electronic structure of the ligand. The data in Table VII are for the highest intensity component of a manifold of low-energy MLCT bands, which can be assigned to $\pi^*(trpy) \leftarrow d\pi(Ru)$ transitions.

In Table VIII are given $E_{1/2}$ values determined by cyclic voltammetry for the salt $[(NH_3)_5Ru(4\text{-CN-}N\text{-Mepy})](PF_6)_3$ in a series of solvents. Data are given for both the metal-based oxidation ($Ru^{III/II}$) and the ligand-based reduction ($pyMe^{+/0}$) waves. It should be noted that the reference electrode used for the electrochemical measurements was the aqueous SCE electrode and that no attempt was made to correct the data for difference in diffusion coefficients of the reduced vs. oxidized species. The relatively slight variation of the ligand-based couple with solvent shows that such effects are negligible, at least within the accuracy with which the data are needed in the discussion which follows.

Table IV. $E_{1/2}$ Values vs. the SCE in Acetonitrile (V)[a]

compd	$E_{1/2}$ ($Ru^{III/II}$)[b]	$E_{1/2}$ ($pyd^{+/0}$)[b]
$[Ru(bpy)_3](PF_6)_2$	+1.29[c]	−1.23
$[Ru(trpy)(bpy)(NH_3)](PF_6)_2$[d]	+1.17	−1.23
$[Ru(bpy)_2(NH_3)_2](ClO_4)_2$	+0.91	−1.48
$[Ru(trpy)(NH_3)_3](ClO_4)_2$	+0.74	−1.53
$[Ru(bpy)(NH_3)_4](PF_6)_2$	+0.51	−1.71
$[Ru(NH_3)_5py](PF_6)_2$	+0.36	
$[Ru(NH_3)_5(4\text{-CN-}N\text{-Mepyd})](PF_6)_3$	+0.77	−0.74
trans-$[(py)Ru(NH_3)_4(4\text{-CN-}N\text{-Mepyd})](PF_6)_3$	+0.83	−0.69
trans-$[(3\text{-Cl-py})Ru(NH_3)_4(4\text{-CN-}N\text{-Mepyd})](PF_6)_3$	+0.97	−0.66
trans-$[(3,5\text{-Cl}_2\text{py})Ru(NH_3)_4(4\text{-CN-}N\text{-Mepyd})](PF_6)_3$	+1.03	−0.63
$[Ru(NH_3)_5(N\text{-Me-4,4′-bpy})](PF_6)_3$	+0.38	−0.93
trans-$[(py)Ru(NH_3)_4(N\text{-Me-4,4′-bpy})](PF_6)_3$	+0.56	−0.89
trans-$[(3\text{-Cl-py})Ru(NH_3)_4(N\text{-Me-4,4′-bpy})](PF_6)_3$	+0.70	−0.88
trans-$[(3,5\text{-Cl}_2\text{py})Ru(NH_3)_4(N\text{-Me-4,4′-bpy})](PF_6)_3$	+0.83	−0.86
$[Ru(NH_3)_5(dmabn)](PF_6)_2$		
$[Ru(NH_3)_5(dmabn)]Cl_3$	+0.18[e]	
$[Ru(NH_3)_5(dmapy)](PF_6)_2$		
$[Ru(NH_3)_5(dmapy)]Cl_3$	−0.14[e]	
$[4\text{-CN-}N\text{-Mepyd}](BF_4)$		−0.69
$[N\text{-Me-4,4′-bpy}](PF_6)$		−0.96

[a] Measured at a polished Pt-disk electrode in 0.1 M TBAH-acetonitrile (except where noted) at 23 ± 2 °C with a sweep rate of 200 mV/s. Ligand abbreviations are given in Table I. [b] ±0.02 V. [c] Taken from ref 24. [d] trpy is 2,2′,2″-terpyridine. [e] Measured at a polished gold-disk electrode in H_2O at 23 ± 2 °C adjusted to 1.0 M ionic strength with a 0.09 M NaTFA and a 0.01 M HOAc–NaOAc pH 5 buffer.

Discussion

A number of significant points are raised by the solvent dependence data reported in the previous section. The approach that we will take in discussing them is as follows: (1) First, we will consider the data in the context of available empirical solvent scales. (2) The data will be considered in the context of charge-transfer theory and comparisons made with related systems. (3) Some practical implications of the data related to selective outer-sphere solvation and the effect of solvent on ion-pair formation will also be considered.

Correlations with Empirical Solvent Scales. The series of polar, aprotic solvents used in this study and a list of the relevant intrinsic physical and empirically derived parameters that characterize them are shown in Table IX. As mentioned in the Introduction, attempted correlation of the MLCT band in $Ru(NH_3)_5py^{2+}$ or in any of the other ammine complexes used in this study with the widely used empirical parameters E_T[7] or Z[8] (see Table IX) showed little agreement.

Attempted single-parameter correlations with intrinsic solvent properties like $1/D_{op}$, $1/D_s$, $1/D_{op} - 1/D_s$, or solvent dipole moment (μ_g) also failed.

In Figures 3–5 are shown plots for a number of the complexes of E_{op} vs. the donor number parameter (DN) defined by Gutmann.[21] The donor number of a solvent, S, is defined as the enthalpy change at 25 °C for the reaction in eq 11 in

$$SbCl_5 + :S \rightleftharpoons Cl_5Sb{\leftarrow}S \qquad (11)$$

1,2-dichloroethane with $[SbCl_5] = 10^{-3}$ M. As such, it presumably measures largely the electron-pair-donor ability or "donicity" of S relative to 1,2-dichloroethane, whose interaction

(20) Preparation of these complexes will be discussed in a forthcoming publication concerning trpy–Ru^{II} chemistry: Sullivan, B. P.; Calvert, J. C.; Meyer, T. J., work in progress.

(21) Gutmann, V. "The Donor-Acceptor Approach to Molecular Interactions"; Plenum Press: New York, 1980.

Table V. Spectral Data for Band Maxima of MLCT Transitions in Various Solvents

solvent	λ_{max}, nm ($\nu_{max}/10^3$, cm^{-1})		
	$[Ru^{II}(NH_3)_5py](PF_6)_2$	$[Ru^{II}(NH_3)_5$-(4-CN-*N*-Mepyd)$](PF_6)_3$	$[Ru^{II}(NH_3)_5$-(4-Me-4,4′-bpy)$](PF_6)_3$
nitromethane (NM)	401 ± 2 (24.94 ± 0.12)	529 ± 2 (18.90 ± 0.08)	561 ± 2 (17.83 ± 0.06)
nitrobenzene (NB)	*a*	545 ± 5 (18.35 ± 0.17)	592 ± 3 (16.89 ± 0.09)
benzonitrile (BN)	412 ± 2 (24.27 ± 0.11)	558 ± 2 (17.92 ± 0.08)	600 ± 2 (16.67 ± 0.06)
acetonitrile (AN)	407 ± 2 (24.57 ± 0.11)	543 ± 3 (18.42 ± 0.10)	584 ± 2 (17.12 ± 0.06)
propylene carbonate (PC)	417 ± 2 (23.98 ± 0.11)	546 ± 2 (18.32 ± 0.07)	600 ± 2 (16.67 ± 0.06)
cyclopentanone (CP)	*a*	562 ± 2 (17.79 ± 0.06)	627 ± 5 (15.95 ± 0.10)
acetone (AC)	418 ± 2 (23.92 ± 0.11)	550 ± 2 (18.18 ± 0.06)	605 ± 2 (16.53 ± 0.05)
N-methylformamide (NMF)	434 ± 2 (23.04 ± 0.11)	577 ± 2 (17.33 ± 0.06)	654 ± 2 (15.29 ± 0.05)
tri-*n*-butyl phosphate (TBP)	431 ± 2 (23.20 ± 0.11)	579 ± 4 (17.27 ± 0.12)	638 ± 2 (15.67 ± 0.05)
dimethylformamide (DMF)	436 ± 2 (22.94 ± 0.11)	581 ± 2 (17.21 ± 0.06)	658 ± 2 (15.20 ± 0.05)
dimethylacetamide (DMA)	439 ± 2 (22.78 ± 0.11)	586 ± 2 (17.06 ± 0.06)	670 ± 2 (14.93 ± 0.04)
dimethyl sulfoxide (Me_2SO)	444 ± 2 (22.52 ± 0.10)	584 ± 2 (17.12 ± 0.06)	672 ± 2 (14.88 ± 0.04)
hexamethylphosphoramide (HMPA)	459 ± 2 (21.79 ± 0.10)	619 ± 2 (16.16 ± 0.05)	729 ± 2 (13.72 ± 0.03)

solvent	λ_{max}, nm ($\nu_{max}/10^3$, cm^{-1})			
	trans-$[(py)Ru^{II}(NH_3)_4$(4-CN-*N*-Mepyd)$](PF_6)_3$		*trans*-$[(py)Ru^{II}(NH_3)_4$(*N*-Me-4,4′-bpy)$](PF_6)_3$	
	MLCT 1	MLCT 2	MLCT 1	MLCT 2
nitromethane (NM)	517 ± 2 (19.34 ± 0.07)		543 ± 2 (18.42 ± 0.06)	*a*
nitrobenzene (NB)	526 ± 2 (19.01 ± 0.07)	*a*	563 ± 2 (17.76 ± 0.06)	*a*
benzonitrile (BN)	538 ± 2 (18.59 ± 0.07)	344 ± 2 (29.07 ± 0.17)	587 ± 2 (17.04 ± 0.06)	
acetonitrile (AN)	525 ± 2 (19.05 ± 0.07)	337 ± 2 (29.67 ± 0.17)	557 ± 2 (17.95 ± 0.06)	376 ± 2 (26.59 ± 0.14)
propylene carbonate (PC)	531 ± 2 (18.83 ± 0.07)	343 ± 2 (29.15 ± 0.17)	569 ± 2 (17.57 ± 0.06)	379 ± 2 (26.39 ± 0.14)
acetone (AC)	537 ± 2 (18.62 ± 0.07)	345 ± 2 (28.99 ± 0.17)	572 ± 2 (17.48 ± 0.06)	383 ± 2 (26.11 ± 0.14)
N-methylformamide (NMF)	554 ± 2 (18.05 ± 0.06)	354 ± 2 (28.25 ± 0.16)	614 ± 2 (16.29 ± 0.06)	394 ± 2 (25.38 ± 0.14)
tri-*n*-butyl phosphate (TBP)	549 ± 4 (18.21 ± 0.13)	350 ± 4 (28.57 ± 0.32)	609 ± 4 (16.42 ± 0.06)	393 ± 3 (25.44 ± 0.20)
dimethylformamide (DMF)	557 ± 2 (17.95 ± 0.06)[b]	354 ± 2 (28.25 ± 0.16)	618 ± 2 (16.18 ± 0.06)	395 ± 2 (25.32 ± 0.13)
dimethylacetamide (DMA)	570 ± 2 (17.54 ± 0.06)[b]	*b*	630 ± 2 (15.87 ± 0.06)	396 ± 2 (25.25 ± 0.13)
dimethyl sulfoxide (Me_2SO)	558 ± 2 (17.92 ± 0.06)	*a*	627 ± 2 (15.95 ± 0.06)	399 ± 2 (25.06 ± 0.12)
hexamethylphosphoramide (HMPA)	583 ± 2 (17.15 ± 0.06)[b]	367 ± 2 (27.25 ± 0.15)	667 ± 2 (14.99 ± 0.06)	407 ± 2 (24.57 ± 0.12)

[a] Peak unobservable due to interfering solvent absorption. [b] The compound decomposed significantly within 5 min.

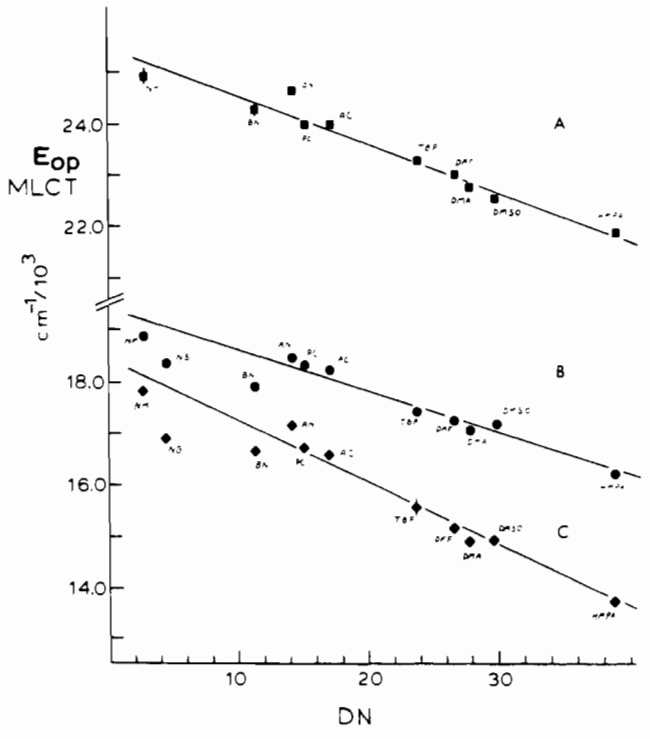

Figure 3. E_{op}(MLCT) vs. donor number for $[(NH_3)_5Ru^{II}py]^{2+}$ (A), $[(NH_3)_5Ru^{II}$(4-CN-*N*-Mepyd)$]^{3+}$ (B), and $[(NH_3)_5Ru^{II}$(*N*-Me-4,4′-bpy)$]^{3+}$ (C).

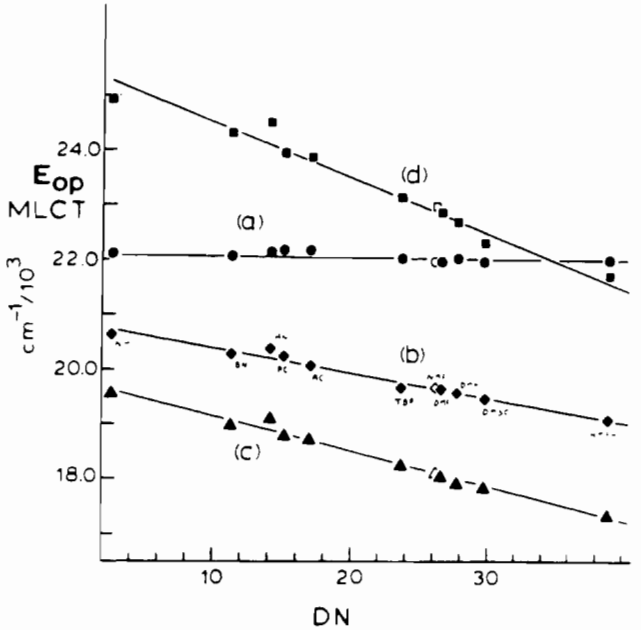

Figure 4. E_{op}(MLCT) vs. DN for a series of complexes with differing numbers of ammine ligands: (a) $[Ru^{II}(bpy)_3]^{2+}$; (b) $[(NH_3)_2Ru^{II}(bpy)_2]^{2+}$; (c) $[(NH_3)_4Ru^{II}(bpy)]^{2+}$; (d) $[(NH_3)_5Ru^{II}(py)]^{2+}$.

with $SbCl_5$ is assumed to be nearly zero.

It is quite clear that the correlations with donor number are successful, and a summary of the correlations, including the correlation coefficient, *R*, for a number of compounds is given in Table X. The data in Table X are summarized by the single linear equation

$$E_{op} = \text{slope} \times \text{DN} + \text{intercept} \qquad (12)$$

The intercepts of the plots are a measure of the energies of the optical transitions in 1,2-dichloroethane, a result that is, in general, unavailable experimentally because of a lack of

Table VI

(a) Spectral Data for the Lowest Energy MLCT Transitions of Some Ruthenium(II) Complexes with Differing Numbers of Coordinated Ammines in Various Solvents

	λ_{max}, nm ($\nu_{max}/10^3$, cm^{-1})		
solvent	$[Ru^{II}(bpy)_3](PF_6)_2$	$[(NH_3)_2Ru^{II}(bpy)_2](PF_6)_2$	$[(NH_3)_4Ru^{II}(bpy)](PF_6)_3$
NM	452 ± 2 (22.12 ± 0.1)	484 ± 2 (20.66 ± 0.09)	511 ± 2 (19.57 ± 0.08)
BN	453 ± 2 (22.08 ± 0.1)	493 ± 2 (20.28 ± 0.09)	527 ± 2 (18.98 ± 0.08)
AN	451 ± 2 (22.17 ± 0.1)	490 ± 2 (20.41 ± 0.09)	523 ± 2 (19.12 ± 0.08)
PC	450 ± 2 (22.22 ± 0.1)	494 ± 2 (20.24 ± 0.08)	532 ± 2 (18.80 ± 0.07)
CP	452 ± 2 (22.12 ± 0.1)	500 ± 2 (20.00 ± 0.08)	531 ± 2 (18.62 ± 0.07)
AC	450 ± 2 (22.22 ± 0.1)	497 ± 2 (20.08 ± 0.08)	534 ± 2 (18.73 ± 0.07)
TBP	453 ± 2 (22.08 ± 0.1)	508 ± 2 (19.69 ± 0.08)	548 ± 2 (18.25 ± 0.07)
NMF	454 ± 2 (22.03 ± 0.1)	507 ± 2 (19.72 ± 0.08)	552 ± 2 (18.12 ± 0.07)
DMF	454 ± 2 (22.03 ± 0.1)	508 ± 2 (19.69 ± 0.08)	554 ± 2 (18.05 ± 0.06)
DMA	453 ± 2 (22.08 ± 0.1)	510 ± 2 (19.61 ± 0.08)	558 ± 2 (17.92 ± 0.06)
Me_2SO	454 ± 2 (22.03 ± 0.1)	513 ± 2 (19.49 ± 0.08)	561 ± 2 (17.83 ± 0.06)
HMPA	453 ± 2 (22.08 ± 0.1)	523 ± 2 (19.12 ± 0.08)	576 ± 2 (17.36 ± 0.06)

(b) Spectral Data for terpy Complexes in Various Solvents

	λ_{max}, nm ($\nu_{max}/10^3$, cm^{-1})			λ_{max}, nm ($\nu_{max}/10^3$, cm^{-1})	
solvent	$[Ru^{II}(trpy)(bpy)(NH_3)](PF_6)_2$	$[Ru^{II}(trpy)(NH_3)_3](PF_6)_2$[a]	solvent	$[Ru^{II}(trpy)(bpy)(NH_3)](PF_6)_2$	$[Ru^{II}(trpy)(NH_3)_3](PF_6)_2$[a]
NM	480 (20.83)	525 (19.05)	TBP	496 (20.16)	558 (17.92)
AN	483 (20.70)	537 (18.62)	DMF	497 (20.12)	566 (17.67)
PC	485 (20.62)	541 (18.48)	Me_2SO	498 (20.08)	572 (17.48)
AC	485 (20.16)	558 (17.92)	HMPA	504 (19.84)	583 (17.15)

[a] Most intense peak in manifold.

Table VII. Spectral Data for LMCT Transitions in Various Solvents

	λ_{max}, nm ($\nu_{max}/10^3$, cm^{-1})	
solvent	$[Ru^{III}(NH_3)_5(dmapy)](PF_6)_2Br$	$[Ru^{III}(NH_3)_5(dmabn)](PF_6)_2Br$
NM	610 ± 20 (16.39 ± 0.39)	862 ± 8 (11.60 ± 0.11)
NB	627 ± 10 (15.94 ± 0.25)	915 ± 20 (10.93 ± 0.23)
BN	583 ± 7 (17.15 ± 0.20)	739 ± 15 (13.53 ± 0.20)
AN	589 ± 5 (16.98 ± 0.14)	791 ± 4 (12.64 ± 0.06)
PC	592 ± 4 (16.89 ± 0.11)	744 ± 3 (13.44 ± 0.06)
CP	561 ± 4 (17.84 ± 0.14)	669 ± 10 (14.95 ± 0.22)
AC	577 ± 5 (17.33 ± 0.15)	716 ± 4 (13.97 ± 0.08)
NMF	537 ± 4 (18.62 ± 0.14)	656 ± 4 (15.24 ± 0.09)
TBP	545 ± 6 (18.35 ± 0.20)	672 ± 3 (14.88 ± 0.07)
DMF	537 ± 3 (18.62 ± 0.10)	656 ± 4 (15.24 ± 0.09)
DMA	527 ± 4 (18.98 ± 0.14)	626 ± 5 (15.97 ± 0.13)
Me_2SO	532 ± 3 (18.80 ± 0.11)	648 ± 5 (15.43 ± 0.12)
HMPA	493 ± 4 (20.28 ± 0.16)	585 ± 5 (17.09 ± 0.14)

Table VIII. Solvent Dependence of the First Oxidation and the First Reduction Waves of $[Ru^{II}(NH_3)_5(4\text{-CN-}N\text{-Mepyd})](PF_6)_3$ (V)[a]

solvent	$E_{1/2}(Ru^{III/II})$	$E_{1/2}(pyd^{+/0})$	$\lvert E_{1/2}(pyd^{+/0}) - E_{1/2}(Ru^{III/II})\rvert$
NM	0.83 ± 0.02	−0.74 ± 0.02[b]	−1.57 ± 0.06
AN	0.77 ± 0.02	−0.74 ± 0.02	−1.51 ± 0.03
PC	0.69 ± 0.02	−0.77 ± 0.02	−1.45 ± 0.03
AC	0.76 ± 0.02	−0.70 ± 0.02	−1.46 ± 0.03
NMF	0.47 ± 0.02	−0.74 ± 0.02[b]	−1.22 ± 0.06
DMF	0.50 ± 0.02	−0.74 ± 0.02	−1.24 ± 0.03
Me_2SO	0.47 ± 0.02	−0.75 ± 0.02	−1.22 ± 0.03

[a] Obtained from standard cyclic voltammograms vs. SCE at 200 mV/s sweep rate with 0.1 M TBAH supporting electrolyte on a polished Pt disk electrode at 23 ± 2 °C. [b] Assumed value.

solubility of the complexes in the solvent. The slopes of the plots provide a measure of the relative sensitivity to variations in the solvent of the two experiments, the energy of the optical transition, and the extent of electron-pair donation to $SbCl_5$.

It is notable that for the MLCT bands, $\pi^*(L) \leftarrow d\pi(Ru(II))$, shown in Figures 3 and 4 the plots of E_{op} and DN have negative slopes, showing that the energy of the optical transition decreases as the electron-donor ability of the solvent increases. As shown in Figure 5, the opposite is true for ligand-to-metal charge-transfer (LMCT) transitions, $d\pi(Ru(II)) \leftarrow \pi(L)$. Slopes of plots of E_{op} and DN are now positive, and E_{op} increases with the electron-pair-donor ability of the solvent.

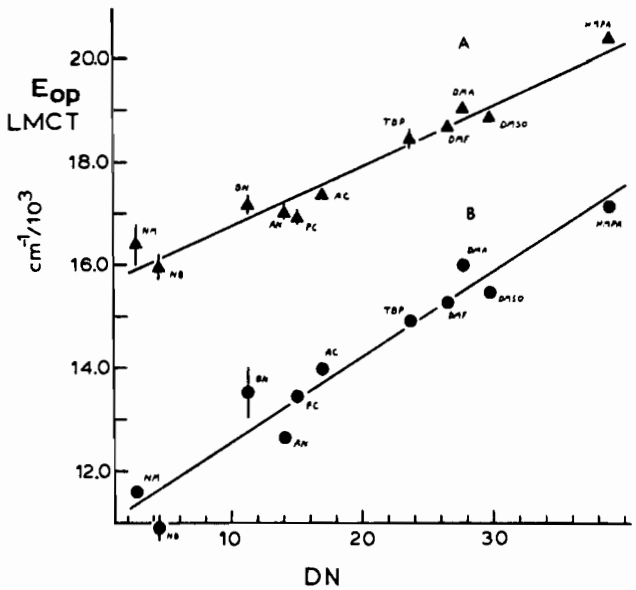

Figure 5. E_{op}(LMCT) for $[(NH_3)_5Ru^{III}(dmapy)]^{3+}$ (A) and $[(NH_3)_5Ru^{III}(dmabn)]^{3+}$ (B).

As a summary statement, it is generally true that good linear correlations ($R \geq 0.94$; see Table X) exist between E_{op} and DN for (1) a variety of π-acceptor ligands including pyridine, polypyridine, or pyridinium ions, (2) both MLCT bands in the complexes *trans*-$Ru(NH_3)_4LL'^{2+}$, and (3) both MLCT and LMCT transitions. In fact, careful inspection of the data in Table X clearly shows that the sensitivity of the optical transition increases as the number of ammine ligands in the coordination sphere increases, regardless of the nature of the π-acceptor ligand. A detailed comparison between the individual cases in Table X is difficult to make because of dif-

Table IX. Solvents and Relevant Parameters from Various Solvent Scales

solvent	D_s[a]	D_{op}[a]	$1/D_{op} - 1/D_s$	μ_g[a,e]	E_T[f]	Z[g]	DN,[b] kcal/mol	β[c]	ΔH_p,[d] kcal/mol
NM	38.6	1.9091	0.498	3.46	46.3		2.7		
NB	34.8	2.403	0.387	4.22			4.4	0.393	
BN	25.2	2.3375	0.388	4.98	42.0		11.9	0.409 ± 0.024	
AN	36.2	1.8066	0.526	3.92	46.0	71.3	14.1		4.2 ± 0.2
PC	65.1	2.0133	0.481	4.98	46.6		15.1		4.53 ± 0.3
CP	13.5	2.0638	0.410					0.537 ± 0.002	5.50 ± 0.09
AC	20.7	1.8413	0.496	2.88	42.2	65.7	17.0	0.495 ± 0.005	5.59 ± 0.08
NMF	182.0	2.0478	0.482	3.83	54.1				6.44 ± 0.08
TBP	7.8	2.0292	0.367				23.7		
DMF	36.7	2.0458	0.462	48.3	48.3	68.5	26.6	0.710 ± 0.009	6.97 ± 0.11
DMA	37.8	2.0609	0.459	3.81	41.0		27.8	0.749 ± 0.008	7.44 ± 0.13
Me_2SO	49.0	2.1815	0.438	3.96	45.0	71.1	29.8	0.752 ± 0.034	7.21 ± 0.08
HMPA	29.6	2.1255	0.437				38.8	0.990 ± 0.024	8.72 ± 0.07

[a] Obtained from values quoted at either 25 or 20 °C: "Handbook of Chemistry and Physics"; CRC Press: Boca Raton, FL, 1980–1981. Gordon, S. A.; Ford, F. A. "The Chemist's Companion"; Wiley-Interscience: New York, 1972. [b] Taken from ref 21. [c] Taken from ref 27. [d] Taken from ref 28. [e] Gas-phase values, except for PC whose value was recorded in benzene solution. [f] Taken from ref 7. [g] Taken from ref 8.

Table X. Linear Least-Squares Fitting Parameters for the E_{op}–Donor Number Plots

molecule	no. of coordinated ammines	slope, E_{op} (cm^{-1})/DN (cm^{-1})	intercept/10^3, cm^{-1}	correln coeff
MLCT[a]				
$[Ru^{II}(bpy)_3](PF_6)_2$	0	0	22.12	0.990
$[Ru^{II}(trpy)(bpy)NH_3](PF_6)_2$	1	−0.0089	21.03	0.967
$[Ru^{II}(NH_3)_2(bpy)_2](PF_6)_2$	2	−0.127	20.86	0.983
$[Ru^{II}(trpy)(NH_3)_3](PF_6)_2$	3	−0.110	19.29	0.988
$[Ru^{II}(NH_3)_4(bpy)](PF_6)_2$	4	−0.183	19.80	0.986
trans-$[(py)Ru^{II}(NH_3)_4$-(4-CN-*N*-Mepyd)$](PF_6)_3$	4			
MLCT 1		−0.169	19.50	0.951
MLCT 2		−0.213	30.32	0.940
trans-$[(py)Ru^{II}(NH_3)_4$-(*N*-Me-4,4′-bpy)$](PF_6)_3$	4			
MLCT 1		−0.257	18.60	0.944
MLCT 2		−0.233	27.56	0.983
$[Ru^{II}(NH_3)_5py](PF_6)_2$	5	−0.274	25.47	0.980
$[Ru^{II}(NH_3)_5$(4-CN-*N*-Mepyd)$](PF_6)_3$	5	−0.231	19.42	0.980
$[Ru^{II}(NH_3)_5$(*N*-Me-4,4′-bpy)$](PF_6)_3$	5	−0.344	18.45	0.990
LMCT[b]				
$[Ru^{III}(NH_3)_5(dmapy)](PF_6)_2Br$	5	+0.327	15.59	0.982
$[Ru^{III}(NH_3)_5(dmabn)](PF_6)_2Br$	5	+0.466	10.93	0.972

[a] The optical transition observed is $d\pi \rightarrow \pi^*(L)$, metal-to-ligand charge transfer. [b] The optical transition observed is $\pi(L) \rightarrow d\pi$, ligand-to-metal charge transfer.

ferences between complexes, such as (1) number of π-acceptor ligands, (2) distance between metal and ligand sites, and (3) extent of metal–ligand delocalization. However, as shown by the plot in Figure 6 of the slopes from the solvent plots vs. number of ammine ligands, the relative sensitivity of E_{op} to changes in the electron donor ability of the solvent increases in a roughly linear manner. The differences between complexes cited above surely contribute to the observed scatter in the plot, but the evidence seems clear that specific solvent–ammine interactions play a major role in accounting for the solvatochromic behavior of the ammine complexes.

In the plot in Figure 6, $Ru(bpy)_3^{2+}$ represents the point for zero ammine ligands and the essentially zero slope is consistent for this complex in which there are no sites for specific interactions on the periphery. However, there *are* systematic variations in E_{op} with solvent for $Ru(bpy)_3^{2+}$ and related complexes. These variations and a rationale for understanding them will be the basis for a future publication. In any case, compared to the effects observed for ammine complexes, the

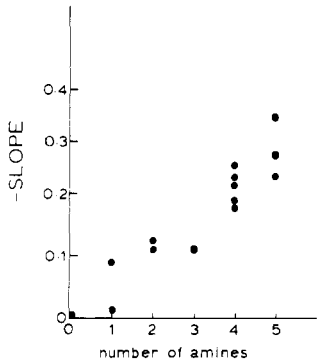

Figure 6. Slopes of E_{op} vs. DN plots taken from Table X vs. the number of coordinated ammines for $\pi^*(L) \leftarrow d\pi(Ru(II))$ absorption bands.

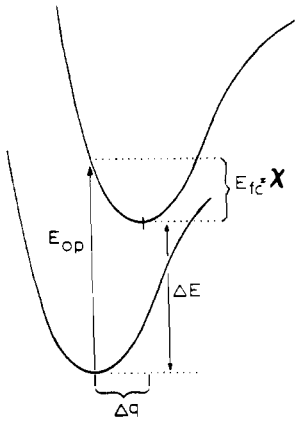

Figure 7. Schematic potential energy diagram illustrating the relationship among E_{op}, χ, and ΔE.

solvent variations for $Ru(bpy)_3^{2+}$ are negligible. The data in Figure 6 show that the sequential replacement of an ammine for a pyridine ligand results in an enhanced sensitivity of E_{op} for the resulting complex toward solvent donicity of ~6%/NH_3 ligand. The total incremental solvent effect can be sizable and can lead to up to 20–30% of E_{op} being determined by solvent. It is this latter quantity that provides the basis for the observed solvatochromism.

Origin of the Solvent Effects. According to charge-transfer theory, E_{op} is given by eq 4, which includes three terms, E_{op}, χ ($=\chi_o + \chi_i$), and ΔE, the internal energy difference between ground and excited states. The relationship among the three terms is shown schematically in Figure 7. Although specific solvent–ligand interactions can influence the character of the intramolecular, normal vibrations, presumably the major

solvent effects will appear in the contributions from the collective vibrations of the medium (χ_o) and in ΔE.

In Table VIII are given the variations with solvent of $E_{1/2}$ values for the metal-based $Ru^{III/II}$ and ligand-based $pyd^{+/0}$ couples for the complex $[(NH_3)_5Ru^{II}NCC_5H_4N^+-CH_3]^{3+}$. The difference in $E_{1/2}$ values, $\Delta E_{1/2} = E_{1/2}(Ru^{III/II}) - E_{1/2}(pyd^{+/0})$, can be related to ΔE, although there are two factors to consider.

(1) By definition, ΔE is the internal energy difference between oxidation-state isomers as shown in eq 8 (note Figure 7). Associated with it is a redox potential difference, $\Delta E_{1/2}$. The experimentally measured $\Delta E_{1/2}'$ value is the free energy change ($-\Delta G$) for the reaction in eq 13.

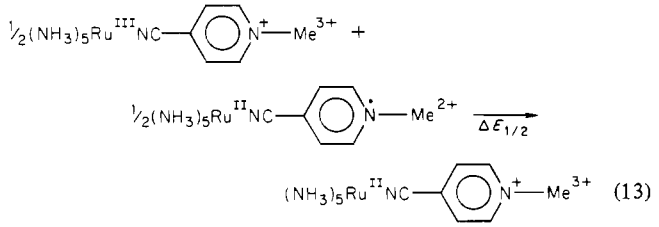

(13)

There will be a difference between $\Delta E_{1/2}$ and $\Delta E_{1/2}'$ because the potentials refer to different reactions. There will be differences between the two arising from both electrostatic and electron delocalization (resonance) effects. It is possible to relate the two on the basis of a simple thermochemical cycle as shown in eq 14. In the limit that the electron-donor and

$$\Delta E_{1/2} = \Delta E_{1/2}' + \frac{e^2}{D_s d} + \Delta\beta \qquad (14)$$

-acceptor sites can be treated as spheres of equal size, the electrostatic term is given by e^2/dD_s, where d is the internuclear separation. In eq 14 $\Delta\beta$ is the change in electron delocalization or resonance before and after charge transfer. From first-order perturbation theory, $\Delta\beta$ is related to ΔE as shown in eq 15, where $\Delta\alpha$ is the change in the extent of mixing

$$\Delta\beta = \beta_2 - \beta_1 = \alpha_2(\Delta E) - \alpha_1(\Delta E) = (\Delta\alpha)(\Delta E) \qquad (15)$$

of electron-donor and -acceptor orbitals before and after charge transfer.

(2) Because $\Delta E_{1/2}$ is a free energy change and ΔE an internal energy change, $\Delta E_{1/2}$ and ΔE are related by eq 16. It

$$\Delta E = \Delta H = \Delta G + T(\Delta S) = \Delta E_{1/2} + T(\Delta S) \qquad (16)$$

seems reasonable that variations in ΔS will make a relatively small contribution numerically.[22]

Combining eq 14–16 gives eq 17, which relates ΔE to the

$$\Delta E = \left(\frac{1}{1-\Delta\alpha}\right)\left(\Delta E_{1/2}' + \frac{e^2}{D_s d} + T(\Delta S)\right) \qquad (17)$$

experimentally obtained redox potential difference between the $Ru^{III/II}$ and $pyd^{+/0}$ couples. Combining eq 17 with eq 4 gives eq 18, which contains the predicted relationship between

$$E_{op} = \chi_i + \chi_o + \left(\frac{1}{1-\Delta\alpha}\right)\left(\Delta E_{1/2}' + \frac{e^2}{D_s d} + T(\Delta S)\right) \qquad (18)$$

E_{op} and $\Delta E_{1/2}'$. Notice that the use of $\Delta E_{1/2}'$ for ΔE in eq 18 leads to an added complexity because of the introduction of the additional terms $T(\Delta S)$ and $e^2/D_s d$ and the change in the extent of electron delocalization. On the basis of eq 18, variations in E_{op} with solvent should be determined by (1) variations in $\Delta E_{1/2}'$, $T(\Delta S)$, and $e^2/D_s d$ with solvent and (2) the variation of χ_o with solvent, which in terms of macroscopic

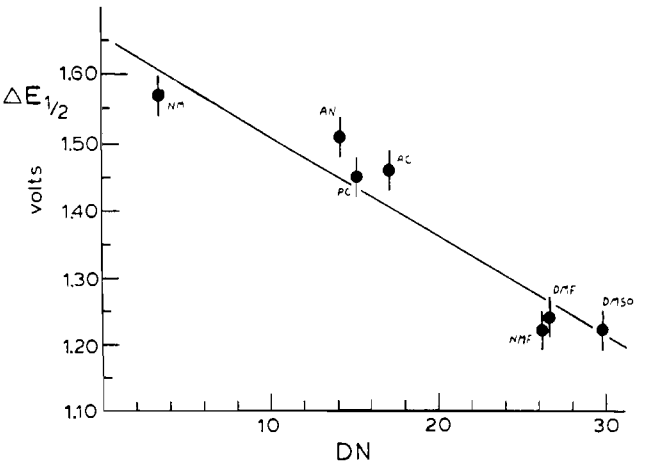

Figure 8. $[E_{1/2}(Ru^{III/II}) - E_{1/2}(pyd^{+/0})] = \Delta E_{1/2}'$ vs. DN for $[(NH_3)_5Ru^{II}(4\text{-CN-}N\text{-Mepyd})]^{3+}$.

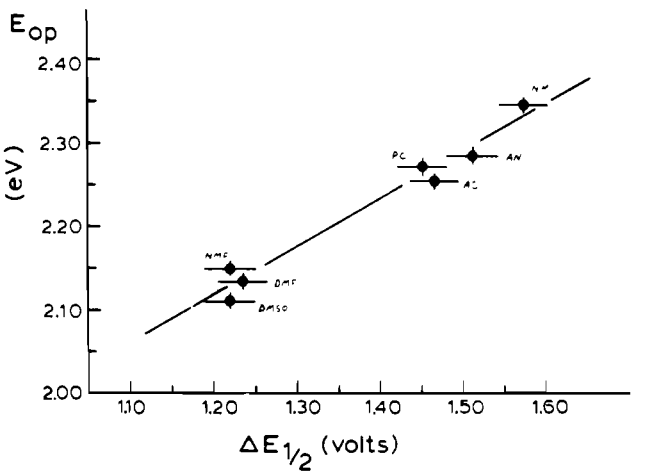

Figure 9. E_{op}(MLCT) vs. $[E_{1/2}(Ru^{III/II}) - E_{1/2}(pyd^{+/0})]$ for $[(NH_3)_5Ru^{II}(4\text{-CN-}N\text{-Mepyd})]^{3+}$.

dielectric continuum theory is predicted by eq 6. It should be noted that eq 6 follows from eq 5 only in the limit that the electron donor and acceptor sites can be treated as spheres of radii a_1 and a_2 with an interreactant separation d between them.

If we return to the redox potential data in Table VIII, it is obvious that the origin of variations in $\Delta E_{1/2}'$ with solvent is almost entirely in $E_{1/2}$ for the Ru(III)/Ru(II) couple. Related solvent effects have also been observed in redox potential measurements for other metal–ammine type complex couples.[23,24] $E_{1/2}$ for the $pyd^{+/0}$ couple is relatively solvent insensitive. Further, as shown in Figure 8, an excellent linear correlation exists between $\Delta E_{1/2}'$ and DN, and as must follow, and as demonstrated in Figure 9, there is also an excellent linear correlation between E_{op} and $\Delta E_{1/2}'$. What this correlation suggests is that, if the model is correct, the $e^2/D_s d$ and $T(\Delta S)$ terms in eq 18 may be relatively small with the solvent dependence in E_{op} coming largely from $\Delta E_{1/2}'$ and specifically from the $(NH_3)_5Ru^{III/II}$ couple.

We have attempted dual-parameter fits[25] to E_{op} using parameters of the type A_1 $(1/D_{op} - 1/D_s)$ and A_2 (DN) in order to include the dielectric continuum prediction for χ_o. The correlation obtained by using a dual-parameter fit is reasonably

(22) Sakami, S.; Weaver, M. J. *J. Electroanal. Chem.* **1981**, *122*, 171–181.

(23) (a) Mayer, U.; Kotocova, A.; Gutmann, V.; Gerger, W. *J. Electroanal. Chem.* **1979**, *100*, 875. (b) See also: Gritzner, G.; Danksagmuller, K.; Gutmann, V. *Ibid.* **1976**, *72*, 177.

(24) Kadish, K. M.; Das, K.; Schaeper, D.; Merrill, C.; Welch, B. R.; Wilson, L. J. *Inorg. Chem.* **1980**, *19*, 2816.

(25) Sullivan, B. P.; Kober, E. M.; Caspar, J. V., manuscript in preparation.

satisfactory, but its statistical meaningfulness is not clear given the limited amount of data available. From the data it is not clear whether or not the theory is applicable for χ_o. Given the existence of relatively strong, specific electron donor pair interactions between solvent and the ammine ligands, a more sophisticated treatment for χ_o is probably warranted. The slope of the line in Figure 8 is only 0.56. According to eq 18, changes in electronic delocalization contribute to the slope but an important contribution could also come from χ_o if it is dominated by specific solvent effects, which also vary with donor number.

Although somewhat ambiguous in its application to the problem of interest here, the treatment given is satisfying from the conceptual point of view. However, as noted above, the solvents used here were nonhydroxylic in character. For solvents like methanol or water, E_{op} values are in poor agreement with the best-fit lines in Figures 3, 7, and 8. It is quite possible that the lack of agreement may signal the onset of strong, specific contributions to χ_o, a point that we are investigating experimentally.

Nature of the Solute–Solvent Interaction. It is possible to develop a reasonably satisfactory qualitative view of the microscopic origins of the dramatic solvent effects observed here, at least for the ΔE term in eq 4 and for $\Delta E_{1/2}'$ from the redox potential measurements. As noted above, the most important solvent contribution to E_{op} is from ΔE ($\Delta E_{1/2}'$), and in particular from the solvent dependence of $E_{1/2}$ for the Ru(III)/Ru(II) couple. A thermochemical cycle for the couple could be written that would include as important terms the differences in solvation energies between the Ru(III) and Ru(II) ions. The dependence of $E_{1/2}$ on DN shows the presence of strong, specific solvent effects and the breakdown of the Born solvation equation, which is based on a static dielectric continuum.

At the microscopic level the solvent effect appears to come from a hydrogen-bonding type of interaction involving electron-pair donation from a solvent molecule or molecules to the N–H bond:

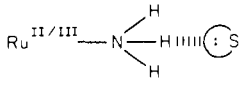

From work in progress, the types of effects observed here are not isolated to complexes containing NH_3 ligands. For example, related effects are observed with Cl^- as ligand although now the variations in CT band energies depend primarily on the *acceptor* properties of the solvent.

H bonding has been described as predominantly an electrostatic interaction that polarizes the closed-shell structures of the participants. The net effect of a hydrogen bond between solvent and an ammine proton is an electron density increase at the metal as can be viewed by the electronic polarizations

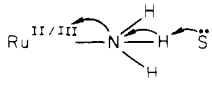

The limiting case is complete loss of a proton and formation of an amido complex

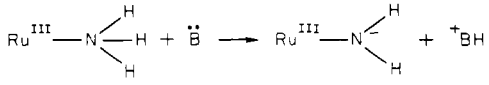

which occurs, for example, for the complex $Ru(NH_3)_6^{3+}$ in basic aqueous solution.[26]

Because of an increased nuclear charge and more acidic NH groups, the stabilization effect of such electron-pair donation

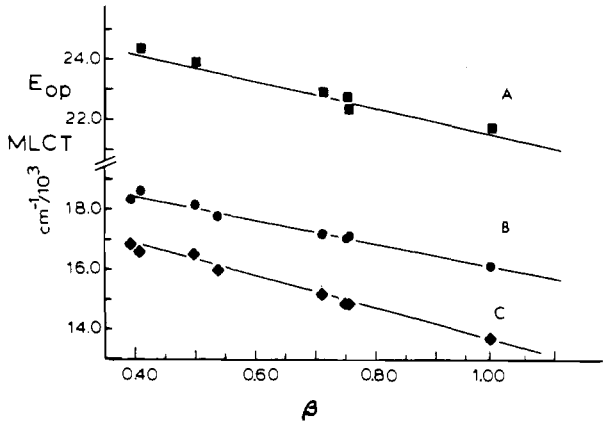

Figure 10. E_{op}(MLCT) for $[(NH_3)_5Ru^{II}py]^{2+}$ (A), $[(NH_3)_5Ru^{II}$(4-CN-*N*-Mepyd)$]^{3+}$ (B), and $[(NH_3)_5Ru^{II}$(*N*-Me-4,4′-bpy)$]^{3+}$ (C) vs. the Taft–Kamlet β parameter.

from solvent will be greater for Ru(III) than for Ru(II) and the effect will increase as donor number increases. With this interpretation, the decrease in ΔE as DN increases arises because of a differential stabilization of Ru(III) by specific electron-pair donation to the N–H bonds of the ammine ligands. The decrease in E_{op} with increasing DN follows immediately because of stabilization of the excited-state oxidation-state isomer $[(NH_3)_5Ru^{III}NCC_5H_4\dot{N}CH_3]^{3+}$ at the expense of the ground state and the fact that E_{op} varies directly with ΔE.

Confirmation of the feasibility of the suggestion comes from the solvent dependence of the LMCT bands, where the sense of the charge-transfer directionality is reversed (see Figure 5 and eq 19 and 20). Here the reversal in charge-transfer

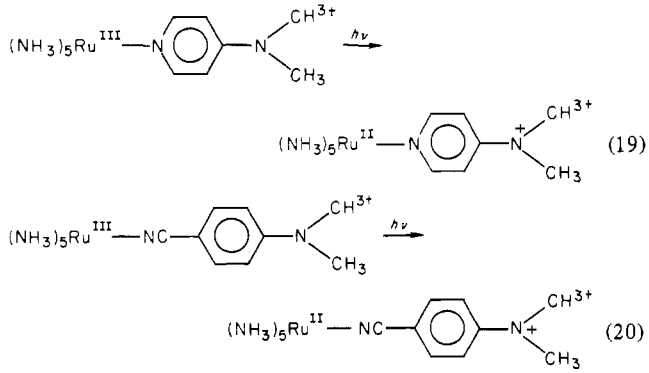

(19)

(20)

direction is reflected in a change of sign in plots of E_{op} vs. DN. The change in sign is consistent with stabilization of the ground state $[(NH_3)_5Ru^{III}$(dmapy)$]^{3+}$, at the expense of the thermally equilibrated excited state $[(NH_3)_5Ru^{II}$(dmapy)$]^{3+}$, that is, once again through ΔE.

Further verification of the importance of hydrogen bonding comes from the excellent correlations of E_{op} with other solvent scales that are based on the hydrogen-bond-accepting ability of the solvent.

One example is the β scale of Kamlet and Taft, which is composite scale of five different indices of a solvent's ability to participate in hydrogen bonding as a Lewis base.[27] Another is the ΔH_p scale of Arnett, which is based on the enthalpy (kcal) of hydrogen-bond formation to *p*-fluorophenol[28] (eq 21).

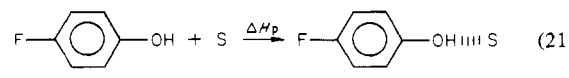

(21)

(26) (a) Navon, G.; Waysbort, D. *J. Chem. Soc. D* **1971**, 1410. (b) See also Waysbort, D.; Navon, G. *J. Phys. Chem.* **1973**, *77*, 960.

(27) Kamlet, M. J.; Taft, R. W. *J. Am. Chem. Soc.* **1976**, *98*, 377.

(28) Arnett, E. M.; Mitchell, E. J.; Murty, T. S. S. R. *J. Am. Chem. Soc.* **1974**, *96*, 3875.

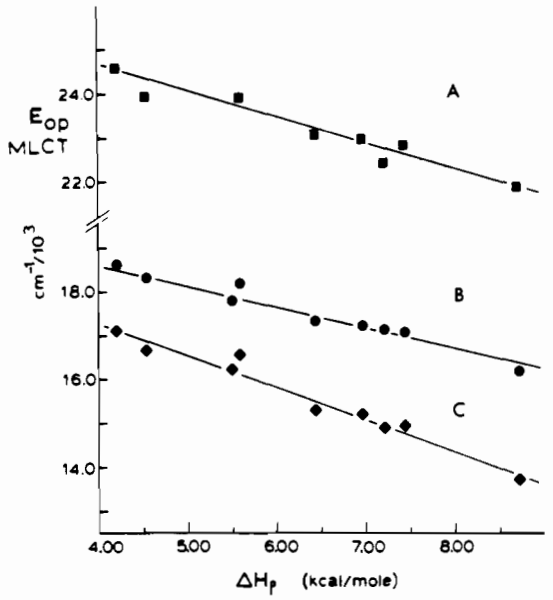

Figure 11. E_{op}(MLCT) for compounds A, B, and C in Figure 10 vs. the ΔH_p parameter.

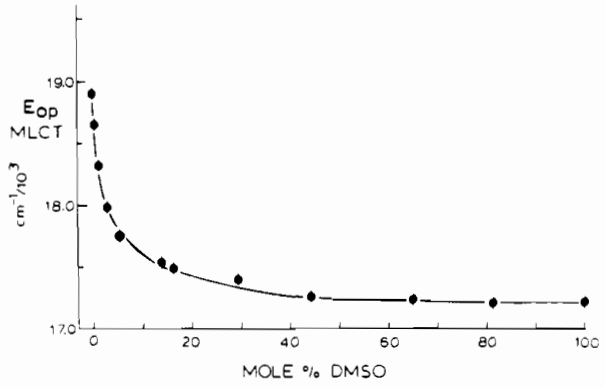

Figure 12. Variation of E_{op} of $[(NH_3)_5Ru(4\text{-}CN\text{-}N\text{-}Mepyd)]^{3+}$ with mole percent Me_2SO in nitromethane.

These parameters have been listed, where available, in Table IX, and in Figures 10 and 11 are shown typical plots of E_{op} of the MLCT bands in $(NH_3)_5Ru^{II}L^{3+}$ (L = 4-CN-*N*-Mepyd and *N*-Me-4,4′-bpy) using the β and ΔH_p scales.

Preferential Solvation and Ion-Pair Formation. One theme that clearly pervades the data presented here is the importance of specific solvent effects arising from electron donation from solvent. In Figure 12 and Table XI are shown the relationships that exist between the energy of the MLCT band in $[(NH_3)_5Ru^{II}(4\text{-}NCC_5H_4N^{+}\text{-}CH_3)]^{3+}$ and the mole percent of Me_2SO (DN = 29.8) present in nitromethane (DN = 2.7). The data are striking and suggest that specific solute–solvent interactions can be sufficient to cause preferential solvation in the outer coordination sphere and that the measurement of CT bands can be a useful experimental probe for exploring such effects. In the pure solvents E_{op} = 529 nm in nitromethane and 583 nm in Me_2SO. From the data in Table XI, it seems apparent that, at a mole fraction of Me_2SO as low as 10%, the effective environment around the complex is nearly that in pure Me_2SO.

Such observations may be of value in studying the role of preferential solvation effects in the study of reaction mechanisms.[29]

(29) (a) Langford, Cooper, H.; Tong, P. K. *Acc. Chem. Res.* **1977**, *10*, 258. (b) Langford, Cooper, H.; Scharte, R.; Jackson, R. *Inorg. Nucl. Chem. Lett.* **1973**, *9*, 1033. (c) Langford, Cooper, H.; Cusumano, M. *Inorg. Chem.* **1978**, *17*, 2222.

Table XI. Charge-Transfer Band Energies for $[Ru(NH_3)_5(4\text{-}CN\text{-}N\text{-}Mepyd)]^{3+}$ in the Mixed-Solvent System Nitromethane–Me_2SO

λ_{max}, nm ($\nu_{max}/10^3$, cm^{-1})	mol % Me_2SO	λ_{max}, nm ($\nu_{max}/10^3$, cm^{-1})	mol % Me_2SO
529 (18.90)	0	567 (17.64)	7.289
536 (18.66)	0.502	573 (17.45)	12.570
546 (18.32)	1.245	575 (17.39)	15.223
556 (17.99)	2.341	578 (17.30)	19.330
563 (17.76)	4.574	583 (17.15)	41.82

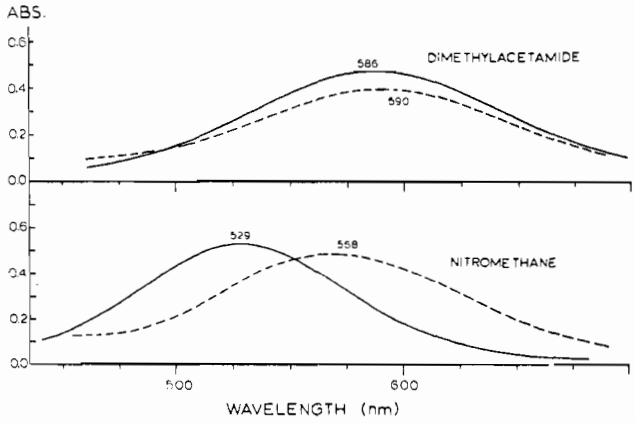

Figure 13. Effect on ion-pair formation between $[(NH_3)_5Ru^{II}(4\text{-}CN\text{-}N\text{-}Mepyd)]^{3+}$ and the iodide ion: (—) 3×10^{-5} M complex; (---) 3×10^{-5} M complex plus 0.033 M tetra-*n*-butylammonium iodide.

A related observation involves the effect of solvent on ion-pair formation. With use of the dielectric continuum theory, the equilibrium shown in eq 22 should depend on the dielectric

$$[(NH_3)_5Ru^{II}N{\equiv}C\text{–}C_6H_4\text{–}NMe]^{3+} + X^- \overset{K_{eq}}{\rightleftharpoons} [(NH_3)_5Ru^{II}N{\equiv}C\text{–}C_6H_4\text{–}NMe, X^-]^{2+} \quad (22)$$

constant of the solvent and the size of the reactants according to simple expressions like the Fuoss equation.[30]

Figure 13 shows the dramatic effect of excess iodide ion on the MLCT band maximum in two solvents of close dielectric constant, nitromethane (ϵ = 38.6) and dimethylacetamide (ϵ = 37.8). In nitromethane a large shift of the MLCT band to lower energy is observed, but in DMA only a slight shift occurs (see Figure 11) even though ion pairing is complete as indicated spectrally.

The clear and dramatic low-energy shift in nitromethane suggests that for the ion pair in this medium, I^- may be acting as an effective electron donor at the NH protons compared to solvent. The effect is expected to be larger in NM than in Me_2SO since Me_2SO is a considerably better donor (DN = 29.8) than NM (DM = 2.7) and can more effectively compete with I^- for the NH groups. It should be noted that in a 0.1 M concentration of added $[CH_3(CH_2)_3]_4N(ClO_4)$ there is no observable effect on the CT band position for $[(NH_3)_5Ru(4\text{-}CN\text{-}N\text{-}Mepyd)]$ in either NM or DMA.

Conclusions and Final Comments

The dramatic solvent effect on metal-to-ligand and ligand-to-metal charge-transfer transition energies in ruthenium(II) and ruthenium(III) ammines has its origin primarily in a solvent-dependent ΔE term. This arises because of specific

(30) Fuoss, R. M. *J. Am. Chem. Soc.* **1958**, *80*, 5059.
(31) Gutmann, V. *Coord. Chem. Rev.* **1976**, *18*, 225.

solvent association at the ammine groups, which is more pronounced when the metal atom has a higher formal charge. The ability of these solutes to act as acceptors leads to solvent–solute and anion–solute effects that are not predicted by an assumption of the medium as a dielectric continuum.

The evidence obtained for preferential solvent-sorting and ion-pairing interactions points out that care must be exercised in interpreting the outer-sphere electron-transfer kinetics involving metal–ammine complexes.

Finally, specific solvent donor–solute acceptor interactions should affect the redox potentials and spectral transition energies in metal complexes involving primary or secondary amines, H_2O, imidazole, and other hydrogen-bond donor ligands, all of which can, in principle, hydrogen bond to solvents.

Acknowledgments are made to the Army Research Office—Durham under Grant No. DAAG29-79-C-0044 for support of this research.

Registry No. $[Ru(bpy)(NH_3)_4](PF_6)_2$, 74887-15-3; $[Ru(NH_3)_5(py)](PF_6)_2$, 72905-29-4; $[Ru(NH_3)_5(4\text{-CN-}N\text{-Mepyd})](PF_6)_3$, 79447-33-9; *trans*-$[(py)Ru(NH_3)_4(4\text{-CN-}N\text{-Mepyd})](PF_6)_3$, 83477-07-0; *trans*-$[(3\text{-Cl-py})Ru(NH_3)_4(4\text{-CN-}N\text{-Mepyd})](PF_6)_3$, 83477-09-2; *trans*-$[(3,5\text{-}Cl_2py)Ru(NH_3)_4(4\text{-CN-}N\text{-Mepyd})](PF_6)_3$, 83477-11-6; $[Ru(NH_3)_5(N\text{-Me-}4,4'\text{-bpy})](PF_6)_3$, 79447-35-1; *trans*-$[(py)Ru(NH_3)_4(N\text{-Me-}4,4'\text{-bpy})](PF_6)_3$, 83477-13-8; *trans*-$[(3\text{-Cl-py})Ru(NH_3)_4(N\text{-Me-}4,4'\text{-bpy})](PF_6)_3$, 83477-15-0; *trans*-$[(3,5\text{-}Cl_2py)Ru(NH_3)_4(N\text{-Me-}4,4'\text{-bpy})](PF_6)_3$, 83477-17-2; $[Ru(NH_3)_5(dmabn)](PF_6)_2$, 83477-19-4; $[Ru(NH_3)_5(dmabn)]Cl_3$, 83477-20-7; $[Ru(NH_3)_5(dmapy)](PF_6)_2$, 83477-22-9; $[Ru(NH_3)_5(dmapy)]Cl_3$, 79447-36-2; NM, 75-52-5; NB, 98-95-3; BN, 100-47-0; AN, 75-05-8; PC, 25511-85-7; AC, 67-64-1; NMF, 123-39-7; TBP, 126-73-8; DMF, 68-12-2; DMA, 127-19-5; Me_2SO, 67-68-5; HMPA, 680-31-9.

Contribution from the Division of Chemical and Physical Sciences, Deakin University, Waurn Ponds, Victoria 3217, Australia, and the Department of Inorganic Chemistry, University of Melbourne, Parkville, Victoria 3052, Australia

Investigation of Reduction and Exchange Reactions of Mercury(II) Phosphine Complexes at Mercury Electrodes in Dichloromethane

A. M. BOND,*[1] R. COLTON,[2] D. DAKTERNIEKS,[2] K. W. HANCK,[1,3] and M. ŠVESTKA[1,4]

Received March 25, 1982

The electrochemical reduction at mercury electrodes of a series of $[HgP_2](ClO_4)_2$ complexes (P = phosphine) has been investigated by using dc and differential-pulse polarography. Data from mercury-199 and phosphorus-31 NMR data are used in conjunction with electrochemical results to aid the interpretation of the electrode processes. In dichloromethane, the charge-transfer step is of unity order. Thus, the polarographic half-wave potential, $E_{1/2}$, is independent of the concentration of either $[HgP_2]^{2+}$ or P, and despite evidence for formation of $[HgP_n]^{2+}$ (n = 2–4) complexes from NMR data, these complexes are not observed at the electrode surface. Instead, the electrochemical data appear as the superimposition of the electrode processes for reduction of the $[HgP_2]^{2+}$ complex and oxidation of the ligand in the presence of mercury to produce $[HgP_2]^{2+}$. A reaction scheme consistent with the observed characteristics of the electrode process is

$$[HgP_2]^{2+} + Hg \rightleftharpoons 2[HgP]^{+} \quad (1)$$

$$2[HgP]^{+} + 2e^{-} \rightleftharpoons 2Hg + 2P \quad (2)$$

to give an overall reaction

$$[HgP_2]^{2+} + 2e^{-} \rightleftharpoons Hg + 2P \quad (3)$$

The large substituent effect observed with different phosphine ligands, and the unusual nature of the electrode process, implies that the presence of mercury(I), or elemental mercury, can catalyze exchange reactions at the electrode surface and modify others. Thus, polarograms for reduction of $[HgP_2]^{2+}$, of $[HgP'_2]^{2+}$ ($P \neq P'$), or of $[HgP_2]^{2+}$ and $2P'$ may be substantially different when both phosphines are present simultaneously compared with polarograms obtained from individual solutions. Electrochemical studies on mixtures of compounds show that the following reactions and probably other second-order exchange reactions are significant at mercury electrodes ($E_{1/2}[HgP'_2]^{2+}$ more negative than $E_{1/2}[HgP_2]^{2+}$):

$$[HgP_2]^{2+} + [HgP'_2]^{2+} \rightleftharpoons 2[HgPP']^{2+} \quad (4)$$

$$[HgP_2]^{2+} + P' \rightleftharpoons [HgPP']^{2+} + P \quad (5)$$

$$[HgPP']^{2+} + P' \rightleftharpoons [HgP'_2]^{2+} + P \quad (6)$$

NMR data confirm the existence of complex exchange reactions, although precipitation of complexes from some mixtures, and the ability of elemental mercury to modify reactions, implies that considerable care is required in the interpretation of the NMR data.

Introduction

Mercury compounds exhibit a wide range of coordination numbers and stereochemistries. Mercury has one isotope, ^{199}Hg, of nuclear spin $^1/_2$ and reasonable abundance, which, with the advent of commercially available Fourier transform NMR spectrometers, allows solutions in the 0.1 M and higher concentration range to be studied readily by mercury NMR to provide considerable information on the nature of species in solution.[5]

Mercury-199 NMR studies on phosphine complexes of mercury(II) have been hampered by the inadequate solubility of many of the complexes, although ^{31}P NMR data can be obtained more readily. Thus, $Hg(PPh_3)_2(ClO_4)_2$ has been examined by ^{31}P NMR methods but not by ^{199}Hg NMR.[6,7]

(1) Deakin University.
(2) University of Melbourne.
(3) On leave from the Department of Chemistry, North Carolina State University, Raleigh, NC.
(4) On leave from the Heyrovský Institute, Czechoslovak Academy of Sciences, Prague, Czechoslovakia.

(5) R. K. Harris and B. E. Mann, Eds., "NMR and the Periodic Table", Academic Press, London, New York, San Francisco, 1978, pp 266–272.
(6) E. C. Alyea, S. A. Dias, R. G. Goel, W. G. Ogini, P. Pilon, and D. W. Meek, *Inorg. Chem.*, **17**, 1697 (1978).

0020-1669/83/1322-0236$01.50/0